AN ABSTRACT OF THE THESIS OF

Bahar Özmen for the degree of Master of Science in Chemistry presented on July 16, 2007

Title: Solution Deposition and Characterization of the Thin Film Inorganic Materials

Abstract approved:

_____

Douglas A. Keszler

The general emphasis of this work has been synthesis, characterization, and applications of n- and p-type inorganic oxide thin films that are deposited from solutions. In particular, a study of n-type transparent semiconductor films of tin (IV) oxide and zinc-doped tin (IV) oxide has been performed by spin coating. Solution deposition of antimony-doped to tin (IV) oxide films was also examined for the production of a conductor.

The solution deposition of p-type cuprous oxide thin films has been achieved by spin coating an aqueous precursor of copper (II) formate tetrahydrate (aq) and annealing under nitrogen atmosphere. UV curing has also been used to prepare the films.

The solution deposition of silver films is performed with the aim of obtaining a conductive contact for a TFT device. Silver metal films were deposited from solutions of $Ag_2O(s)$ in aqueous ammonia by spin coating method and annealing in air at temperatures as low as 120^0C.

©Copyright by Bahar Özmen
July 16, 2007
All Rights Reserved

Solution Deposition and Characterization of the Thin Film Inorganic Materials

by
Bahar Özmen

A THESIS

submitted to

Oregon State University

in partial fulfillment of
the requirements for the
degree of

Master of Science

Presented July 16, 2007
Commencement June 2008

Master of Science thesis of Bahar Özmen
presented on July 16, 2007

APPROVED:

Major Professor, representing Chemistry

Chair of the Department of Chemistry

Dean of the Graduate School

I understand that my thesis will become part of the permanent collection of Oregon State University libraries. My signature below authorizes release of my thesis to any reader upon request.

Bahar Özmen, Author

ACKNOWLEDGEMENTS

First, I would like to thank to my family members including my mom, Esma Özmen, my dad, Mehmet Ali Özmen, my sister Çiğdem Özmen and her family for their encouragement and support throughout my career. They are the people who make it possible to live a happy childhood and taught me the tough sides of the life. I experienced the happiness and joy in a family with them. Who I am today, has been most influenced by their emotional support and their courage which helped me to take my degrees successfully. Especially my dad strongly supported me in all my decisions that I made throughout my life. My sister's two lovely sons, one year old Demircan Demir and seven year old Özgür Demir are the joys and cheerful sides of my life.

Another important person in my life is my dear husband Mehmet Murat Monkul, who is my most valuable person in my life. I would like to thank him for being so patient and giving valuable suggestions about everything that bothers me. We did a lot of helpful discussions about our life, my career, our family and everything. Thank to him for being so kind and thoughtful to me all the time and of course for giving me his endless love. He is the person who can make me smile in the worst days of my life. In this life journey I always hope to be together by sharing his successes, happiness as well as his hard times in life.

Thanks are due my advisor, Dr. Douglas A. Keszler for his guidance, experience and valuable ideas in my research. His support financially made this research possible.

I am thankful to Morgan Ferguson for her help in the AFM measurements, to Paul Newhouse for his resistivity measurements on my films and to Dr. Wager's group members for their electrical characterization on my films.

Finally I would like to thank all the current Keszler group members for their patience and their helps including how to use the instruments in my research and valuable discussions together with ideas which helped me a lot in my study. Also their energy and motivation in our frisbee games that made Corvallis more fun for me.

TABLE OF CONTENTS

LIST OF FIGURES

LIST OF FIGURES (Continued)

Figure Page

LIST OF TABLES

Solution Deposition and Characterization of the Thin Film Inorganic Materials

Chapter 1

Introduction

The main scope of this thesis is the solution-based deposition of inorganic materials by spin coating. Solution-based processing is applicable to many organic and polymeric materials, but the electronic devices fabricated with these materials exhibit modest performance; films and devices from inorganic precursors exhibit higher performance (Anderson J.T., et al, in press, Mitzi D.B., 2004). In this study, deposition of oxide-based inorganic materials is emphasized for low-cost electronics by solution-based, environmentally friendly, and vacuum-free fabrication in the production of chemically robust materials and devices.

In this study, straightforward beaker chemistries, nontoxic water-based precursors and, as a deposition method, vacuum-free spin coating are selected. By spin coating, it is possible to obtain films with thicknesses over a very wide range (<10 nm- >1μm). In this technique, a high speed rotation (3000-5000 rpm) is used to spread the fluid by centrifugal force. The selected solvent is usually volatile and evaporates at the time of application. The film thickness is dependent on the concentration of the solution, the type of the solvent, and the spinning speed selected. Usually higher spin rates produce thinner films.

In Chapter 2, the depositions of tin (IV) oxide and zinc-doped tin (IV) oxide semiconductor oxide films have been studied, and progress toward realizing a TFT are discussed. Tin (IV) oxide is studied as a crystalline TFT channel layer due to its many advantageous properties such as its high transparency, high conduction, high chemical stability even at high temperatures, high hardness and adherence to many types of substrates (Gordon R.G., 1996). SnO_2 has uses in high efficiency solar cells, transparent electrodes, gas detectors, far infrared detectors (Munnix S., et al, 1982). Zinc-doped tin

(IV) oxide (ZTO) is also a useful material for many reasons. First, it provides an amorphous nature and a low processing temperature compared to high processing temperatures of crystalline oxide channels. ZTO shows improved transistor performance because of its high electron mobility (30 cm^2/Vs at 500^0C) (Hong D., et al, 2006) in spite of its amorphous character. It has many attractive properties as Minami, et al. concluded, ZTO film ($ZnSnO_3$) showed superior properties as compared with SnO_2 and ZnO, such as the zinc-stannate films were more thermally stable in hydrogen environment than SnO_2 films and are chemically stable in acidic and basic solutions than ZnO films (Minami T., et al., 1995). ZTO shows extreme resistance to scratching (Chiang H.Q., et al, 2005), and more importantly forms an exceedingly smooth surface in thin films (Young D. L., et al., 2002).

In Chapter 2, the deposition of a Sb-doped SnO_2 film from solution is also discussed, since it is a good conductor that can be used as a conductor in a TFT. The high conductivity of Sb-doped SnO_2 film compared to undoped SnO_2 comes from the extra electron on antimony, which is added to the conduction band of SnO_2.

In Chapter 3, the solution deposition of Cu_2O films from a water-based copper (II) formate precursor is described. The aim here is to deposit a p-type channel layer for a TFT from solution.

The materials tin (IV) oxide, zinc-doped tin (IV) oxide and Sb-doped tin (IV) oxide in chapter 2 are the examples of n-type semiconductor transparent conductive oxides (TCOs) where cuprous oxide is a p-type TCO which is discussed in chapter 3. In most of the spin-coated TFT channel layers electronic transport has been n-type which is dependent on the type of semiconductor selected. However, studying p-type channels is also interesting because of their attractive application areas like solar cells, which are based on the formation of a junction between n- and p-type layers (to drive charge separation at the interface). The presence of both n- and p-type transistors is also critical for the complementary metal-oxide semiconductor (CMOS) technology (Mitzi et al, 2006). The preparation of TCO thin films consisting of p-type semiconductors was first reported in 1993 (Sato H., et al, 1993). After this report, which was on p-type NiO thin

films deposited by rf magnetron sputtering, there have been many reports on the preparation of p-type semiconducting thin films using new TCO semiconductors, however there is no report on the preparation of a p-type TCO thin film suitable for use as a practical transparent electrode (Minami T., 2005).

TCO thin films find use in transparent electrodes and can be either polycrystalline or amorphous in structure. They exhibit a resistivity of the order of 10^{-3} Ω cm or less and an average transmittance of the order of 80% in the visible range (Minami T., 2005). In most solids, simultaneous occurrence of high transparency to visible radiation and high electrical conductivity is not common. However, for a small class of post-transition metal oxides with band gaps near 3 eV, good conductivities are possible at low carrier concentrations together with their relatively low absorption in the visible portion of the spectrum (Cava R.J., et al, 1994). Some examples of these TCOs are In_2O_3:Sn (ITO), ZnO:Al and SnO_2:Sb (Hosono H., et al, 1996). Especially Sn-doped In_2O_3 (ITO) is in wide use for many applications. Although the resistivities of transparent films of ITO are quite low, which are in the range of 200-400 μΩ cm, strong absorption in the blue and green limits the thicknesses of 'transparent' films to 2000 Å or less (Jarzebski Z.M., 1982). New materials with improved transparency and good conductivity would be in interest for the rapidly growing areas like flat panel optical displays (Cava R.J., et al., 1994).

Generally, TCOs are interesting for their electro-optical, interfacial, and material compatibility properties (Ginley D. S., et al, 2000). Considering application areas of TCOs, one would understand better why these materials are in high demand. Their wide range of applications include heat collectors, gas sensors, energy conserving (low-emissivity) windows (eg: oven windows, building windows), automatically dimming rear-view mirrors for automobiles and electrically-controlled "smart" windows, transparent electrodes on flat panel displays, solar cells, and touch panels. Among these application areas, a primary application of TCOs is in the form of thin films that are used in TFT-based displays. These displays have a transistor for each pixel on the screen, allowing the electrical current that illuminates the display to be turned on and off at video

rates. Liquid crystal displays (LCDs) that use TFT technology are called "active-matrix" displays, which are higher-quality than older "passive-matrix" displays.

In Chapter 4, the deposition of silver metal from solution, which finds application as a conductor in a TFT, device is discussed. In the TFT devices generally evaporated aluminum metal, gold or ITO are used for the source and drain contacts. Low-cost, solution-processed and conductive silver materials are interesting if a low-temperature deposition method can be applied. Also, by printing nanoparticulate suspensions of gold, silver, and other metals, it is possible to form conductors for electronics applications, and electrodes can be formed by printing a metal precursor solution then converting it to a metal (Calvert P., 2001).

The motivation of this thesis was a functioning TFT device by using the known basic chemistries of the oxides, used in the channel layers. To be able to understand how these devices are functioning first of all the basic parts that a transistor consists of will be discussed. A transistor has four main parts named transistor gate (bottom gate), dielectric (insulator), channel layer, and metal contacts (source and drain). These parts are shown schematically in Figure 1.1. The materials used for the devices described in this work are silicon substrate for the gate, thermally grown SiO_2 for the dielectric, spin-coated semiconductor channel material, and evaporated aluminum for the source (S) and drain (D) contacts.

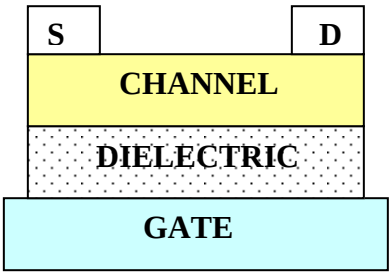

Figure 1.1 Bottom gate TFT layout with the gate at the bottom, dielectric and channel layers with the source and drain contacts on top of it.

The operation of a transistor can be described in terms of electrons flowing from source to drain. The source terminal derives its name from the carriers contributing to the current moving from the external circuit into the semiconductor at this electrode. The carriers leave the semiconductor, or are “drained” from the semiconductor at the drain electrode. The gate is so named because of its control or gating action. The drain current (I_D), which flows in response to the applied terminal voltages, is the primary drive current observable. The current flow is always such that carriers (electrons) enter the structure through the source, leave through the drain, and are subject to the control and gating action of the gate (G). The voltage applied to the gate relative to ground is V_G, while the drain voltage relative to ground is V_D (Pierret R.F., 1996).

For all the chapters considered in this thesis obtaining high quality thin-films was the ultimate goal. These films are useful for mechanical and electrical applications especially for the channel layers used in TFTs. For solution-processed films, in general, atomic rearrangements during solvent loss and annealing generate rough surfaces and incomplete coverage (Anderson J.T., et al., in press). To obtain thin films from solution deposition, two common routes are commonly used. The first one is the deposition of the films by sol-gel method, and the second one is the deposition of the films from rapid condensation of a polymer-gel. In traditional sol-gel deposition, it is difficult to obtain a homogeneous film layer either by very slow hydrolysis and diffusion or by burning organics through a rapid combustion step. In this method, basically a colloidal suspension is converted to a solid-form gel in appropriate viscosity of application to a substrate. The gel can be chemically purified, deposited, and fired at high temperatures into a solid oxide film. There are considerable disadvantages of using the high-temperature burnout step, which leads to significant volume changes and crystallization (Anderson J.T., et al., in press). Moreover the film obtained from this technique commonly appears as a porous film containing extensive void regions as a result of film crystallization. This type of film morphology is not preferred in a channel layer of a TFT device which brings limitations on the device performance. An advantage of using the sol-gel technique is its capability of coating of complex shapes and large surfaces. The conductivity in undoped oxide films

deposited by this technique is generally low (1-10 $ohm^{-1}cm^{-1}$). However, the films are useful for applications that do not depend on high conductivity, but do benefit from cost-effective deposition. For example, fluorescent lamp envelope coatings and transparent grounding films in cathode ray tubes are fabricated by this technique (Brinker C.J., et al., 1990).

The second deposition method which is used in this study is called prompt inorganic condensation. It is the condensation of a gel that produces inorganic oxide thin-films with the lack of complex organic ligands. Condensation reactions form from aqueous metal precursors having metal-hydroxo-metal (M-OH-M) bonds that energetically prefer to produce an inorganic oxide thin-film containing covalent metal-oxo-metal (M-O-M) bonds by giving off water. In this rapid condensation method bonding in the precursor solution is quite important for the production of thin-films. An example of a film deposited by this type of chemistry is shown in Figure 1.2. In this figure a hafnium oxide sulfate ($HfO_{2-x}(SO_4)_x$) film is seen which possesses a dense, uniform, pore and crack-free morphology which is deposited on Ta metal.

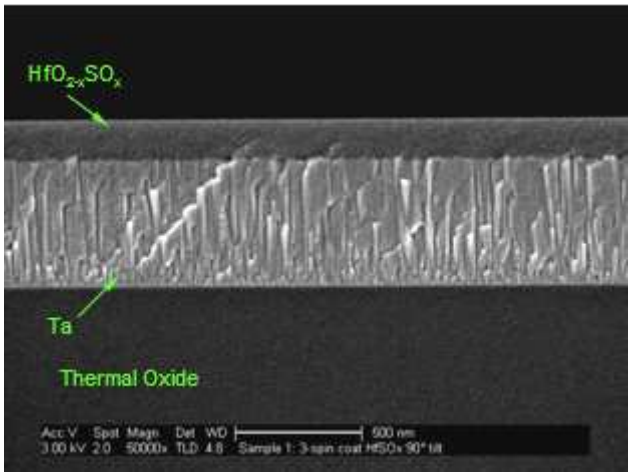

Figure 1.2 Solution processed $HfO_{2-x}(SO_4)_x$ film on a thermal oxide substrate with Ta metal on top of it.

The previously mentioned hydrolysis and condensation reactions with metal-organic precursors are quite slow, which limits the applicability of printing techniques. They also possess an unnecessary expense. The alternative to organic precursors is the use of inorganic precursors, which can be rapidly converted to oxide thin films and at the same time present suitable routes for digital printing.

Thin Films of SnO_2 and Zn-doped SnO_2

Chapter 2

Abstract

Channel-layer performance of tin oxide and zinc-doped tin oxide semiconductor oxide films have been studied by fabricating thin film transistors (TFTs) via spin coating. Electrical characterization of undoped tin (IV) oxide and zinc doped tin (IV) oxide thin films are performed. X-ray diffraction and scanning electron microscope imaging of solution-deposited thin films of tin oxide and zinc-doped tin oxide (ZTO) are taken as a guide for understanding the difficulties in producing functional thin film transistors. IR analysis of SnO_2 films is performed to determine the decomposition temperature of the nitrate present in the films and the temperature at which hydroxide is evaporated from the films. The chloride and zinc percentages present in the films at selected anneal temperatures are determined by electron microprobe analysis. The resistivity of antimony-doped tin oxide from solution is compared with the undoped tin (IV) oxide.

A precursor prepared from tin (II) oxalate, HNO_3 (aq), and H_2O_2 (aq) is examined for depositing tin (IV) oxide films.

Introduction

In this study, I examined the solution-deposited precursors for deposition of undoped and zinc-doped tin (IV) oxide channel layers for use in transparent thin-film transistors (TTFTs). A unique hydroxo nitrato precursor was produced from $SnCl_4.5H_2O$ for realization of SnO_2; this same precursor was slightly modified to produce films of zinc- and antimony-doped SnO_2. To examine the production of highly dense films,

processing was extended to include SnC_2O_4 as a precursor following addition of HNO_3 (aq) and H_2O_2 (aq).

The TTFT represents the fundamental active device in the field of transparent electronics. Such TTFTs were initially fabricated on the basis of crystalline oxide channels resulting from high-temperature processing (above 600^0C, Chiang H.Q. et al, 2005). To reduce these temperatures and improve device performance, amorphous channel layers have been examined (Chiang H.Q., et al, 2005, Hosono H., 2006).

SnO_2 adopts a tetragonal rutile structure (space group $P4_2/mnm$). The unit cell contains two tin and four oxygen atoms. Each tin atom is bound to six oxygen atoms at the corners of a regular octahedron, and every oxygen atom is surrounded by three tin atoms at the corners of an equilateral triangle (Hartnagel H.L., et al, 1995). The value of the direct band gap has been estimated to be 3.6 eV (Munnix S., et al, 1982).

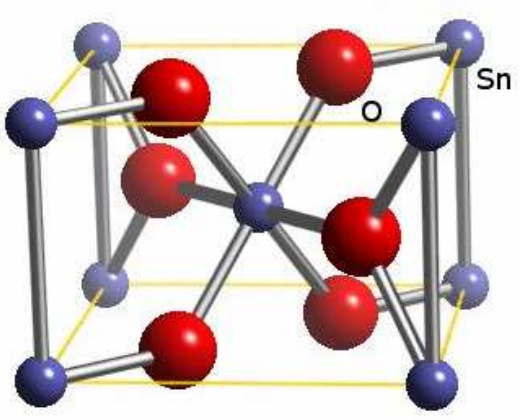

Figure 2.1 Unit cell of the crystal structure of SnO_2. Large circles indicate O atoms and the small circles indicate Sn atoms.

If SnO_2 were completely stoichiometric, it would be expected to be electrically insulating. The material, however, is nonstoichiometric, being anion deficient through the formation of oxygen vacancies. These vacancies lead to reduction of the Sn^{4+} cation and

occupation of the $5s^0$ conduction band. The creation of very high oxygen vacancies results in structural and stoichiometric changes from SnO_2 to SnO. X-ray studies reveal that there are many intermediate oxidation states, such as Sn_2O_3 or Sn_3O_4, which result during conversion of SnO_2 to SnO (Hartnagel H.L., et al, 1995). Undoped SnO_2 films are n-type semiconductors. High conductivity can be induced in SnO_2 films from stoichiometric deviation (tin interstitials and mainly oxygen vacancies), intentional doping (with fluorine and antimony), and unintentional doping (with chlorine when tin chloride compounds are used as reagents for deposition). Substitutional and interstitial chlorine gives rise to donor levels that increase the carrier concentration and conductivity (Bilgin V., et al, 2004). A stoichiometric SnO_2 crystal can be made conducting by creating oxygen deficiencies on heating the sample in a slightly reducing atmosphere. Similarly, replacement of Sn^{4+} with a cation of valence higher than 4+ increases the n-type conductivity, while replacement of Sn^{4+} with a lower valency cation produces a hole, which acts as a trap to decrease the conductivity (Hartnagel H.L., et al, 1995). The combination of a large band gap and high conductivity (associated with high dopant concentrations) makes SnO_2 a useful transparent conductor (Gordon R.G., 1996).

Zinc tin oxide is a wide band gap, n-type semiconductor, and in thin-film form it exhibits optical gaps of 3.3 to 3.9 eV (Minami T., et al, 1995). It has many attractive properties, including chemical stability with respect to oxidation and etching (Minami T., et al, 1995), and physical robustness with resistance to scratching (Chiang H.Q. et al, 2005). Although the electrical properties of doped-SnO_2 (generally doped TCOs) are strongly dependent on the deposition method as well as the deposition conditions, it is possible to obtain low resistivities on the order of 10^{-5} Ω cm with Zn-doped binary compounds (Minami T., 2005). According to Bilgin et al, crystalline structure of the SnO_2 films was deteriorated with increasing Zn concentration which is evident from the decrease in intensity and the number of X-ray peaks for SnO_2. As a result of Zn addition to crystalline SnO_2 films the ZTO film exhibits amorphous structure. Despite the amorphous nature of ZTO it shows mobilities as high as 30 cm^2/Vs (Kluth O., et al, 2003) in the TFT devices. Such high mobilities in an amorphous material can be

explained by the conduction band derived from spherically symmetric ns orbitals of heavy-metal cation. Such orbitals have high degree of overlap between adjacent orbitals and considerable band dispersion (Chiang H.Q., et al, 2005). Zinc addition to thin films of tin oxide is also known to produce smoother surfaces compared to crystalline and granular undoped SnO_2 (Young D. L., et al, 2002).

Experimental

Tin oxide films are obtained upon precipitating a tin (IV) hydroxide gel by slow addition of 0.6 mL concentrated NH_3 (aq) (28-30%, Mallinckrodt Chemicals) to 4.45 mL, an aqueous solution of 0.9 M $SnCl_4.5H_2O$ (98%, Alfa Aesar). The hazy solution is stirred for approximately 30 min at room temperature until it becomes transparent. An additional 1.3 mL concentrated NH_3 (aq) is then added quickly to force precipitation. The gel is centrifuged for 2 min and then washed with a refrigerated 5/2 by volume, ethanol/ water mixture. The washed gel is then centrifuged for a second time for 7 minutes. The separated gel is removed from the liquid and then transferred to a beaker and dissolved in 2.25 mL of 2 M HNO_3 (aq) (68-70%, EMD). The mixture clarifies and becomes transparent after stirring at room temperature for approximately 1 h. This solution is taken as the spin-coating precursor following addition H_2O_2 (aq) (30% solution, Mallinckrodt, Sn: H_2O_2 ~ 1:4). The mol ratio of Sn to HNO_3 is calculated from the molarities previously mentioned and the amounts of $SnCl_4.5H_2O$ (aq) and HNO_3 (aq) added to the solutions. The Sn:NO_3 ratio is thus based on the complete precipitation of Sn^{4+} (aq) following the first addition of NH_3 (aq). In order to quantitatively identify the chloride present in the SnO_2 films Ag (s) (99.99%, Cerac, 325 mesh) is added to the spin coating solution in the mol ratio of Sn:Ag= 0.001:1.

Thin films of tin (IV) oxide are spin-coated on 2000 Å SiO_2/Si substrates that were cleaned for 60 min at 45^0C in an ultrasonic bath containing Conrad 70. The substrates are washed with millipore water and dried by blowing N_2 (g) on them. The transparent spin coating precursor of tin (IV) hydroxo nitrate is deposited by spinning at a rate of 3000 rpm for 30 s and curing on a hot plate at 120^0C for 30 s between each coat. The last anneal temperature of the film is 600^0C for 1 h in air with 10^0C/ h heating and cooling rates.

SnO_2 thin films are also spin coated from a chloride-free tin precursor. 0.21 g of SnC_2O_4 (98%, Avocado) solid is stirred in 2 M HNO_3 (aq), 3 M H_2O_2 (aq), and 6 mL of millipore H_2O in the mol ratios of 1:1:8.5 of SnC_2O_4:HNO_3:H_2O_2. The films are cured at

400^0C between coats, which is the decomposition temperature of the oxalate group. Another precursor is made by addition of 0.2 g SnC_2O_4 (s) to 1 M HCl (36.5-38%, EMD), conc. H_2O_2 (aq), and 3 mL millipore H_2O. The mol ratios used are 1:1.12:30.8 for SnC_2O_4: HCl: H_2O_2.

Zinc-doped SnO_2 films are prepared by using hydroxo nitrato precursor described above, except 0.0793 g of Zn metal (99.9%, Alfa Aesar) (10.5% of Zn/Zn+Sn) was added to the clear spin-coating solution. The dissolution of zinc metal is promoted by the addition of 1.5 mL of 2 M HNO_3 (aq) while stirring. The calculated mol ratio of Sn to HNO_3 is 1:1.69 (does not include the reaction of Zn with HNO_3). The last anneal was 600^0C for 1 h in air with 10^0C/ h heating and cooling rates.

For preparation of Sb:SnO_2, 0.027 g of antimony metal (99.995%, Cerac, 200 mesh) is added to 5 mL of 0.9 M $SnCl_4.5H_2O$ (aq) solution in the mol ratio of Sb:Sn =1:20 by stirring 18 h. 0.3 mL of concentrated NH_3 (aq) and 0.28 mL of millipore water were added to 2.23 mL of this solution, resulting in a hazy solution. It is then stirred for 15 min to produce a clear solution; 1.13 mL of concentrated NH_3 (aq) is then quickly added to obtain a tin antimony hydroxide gel. The solution is centrifuged for 7 min, washed with a mixture of 2.5 mL ethanol and 1 mL millipore water, and then centrifuged a second time for 2 min. After separation of the liquid from the gel, the gel is dissolved with stirring in 1.13 mL of 2 M HNO_3 (aq) over a period of 3.5 h. The calculated Sn:HNO_3 and total metal (Sb+Sn):HNO_3 mol ratios are 1.73:1 and 1.82:1 respectively. (These ratios are derived on the basis of complete and stoichiometric precipitation during gel formation.) The resistivities of the Sb-doped SnO_2 films are measured by van der Pauw method via putting four stainless steel contacts on the films.

Thin-film X-ray diffraction data were collected with a Rigaku/MSC Rapid diffractometer, employing Cu Kα radiation generated from a rotating anode at 50 kV and 270 mA. Electron microprobe analysis (EMPA) data were collected on a Cameca SX-50 electron microprobe spectrometer. Data were collected at three different accelerating voltages with experimental intensities determined from the average of five positions on each sample. Atomic force microscopy in contact mode is used for the identification of

the surface morphologies, and SEM measurements are done at the Hewlett Packard, Company in Corvallis, OR.

Results and Discussion

Ideal reactions that may occur during the deposition of tin (IV) oxide films are listed in reactions 2.1, 2.2 and 2.3. The first step, 2.1, represents precipitation of a tin (IV) hydroxide gel from a tin chloride salt. The second reaction is the dissolution of the resulting gel in HNO_3 (aq) to obtain a soluble tin hydroxo nitrato precursor in solution. The precursor is prepared in this way to minimize the NO_3^- concentration, which hinders condensation. The third reaction occurs after the precursor has been applied to the substrate and thermally annealed.

$$SnCl_4(aq) + 4NH_3(aq) + 4H_2O(l) \longrightarrow Sn(OH)_4(gel) + 4NH_4Cl(aq) \qquad 2.1$$

$$Sn(OH)_4(gel) + xHNO_3(aq) \longrightarrow Sn(OH)_{4-x}(NO_3)_x(aq) + xH_2O(l) \qquad 2.2$$

$$Sn(OH)_{4-x}(NO_3)_x(aq) \longrightarrow SnO_2(s) + xNO_2(g) + (x/4)O_2(g) + ((4-x)/2)H_2O(l) \qquad 2.3$$

As noted above, preparation of the tin (IV) oxide precursor solution is effected by the precipitation of a hydroxide gel via the addition of NH_3 (aq) to $SnCl_4 \cdot 5H_2O$. By heating from 200 to 1000^0C the lattice parameter of SnO_2 is known to decrease, suggesting the presence of a large amount of hydroxyl groups in the SnO_2 crystallites,

which are expelled as H_2O on heating. Large amount of hydroxyls remaining in the bulk of crystallites give rise to a considerable amount of tin vacancy sites. It is also claimed that remaining hydroxyls create structural deformation and bond length variations in rutile structure (Toledo-Antonio J.A., 2003).

One of the issues associated with preparation of the hydroxo gel, reaction 2.1, is the undesired retention of Cl^-. A common test for the presence of Cl^- (aq) in a solution is precipitation of AgCl (s) by addition of Ag^+ (aq). Adding excess silver metal to the dissolved gel and drying it at 300^0C results in the formation of AgCl (s) as noted from the XRD patterns in Figure 2.2.

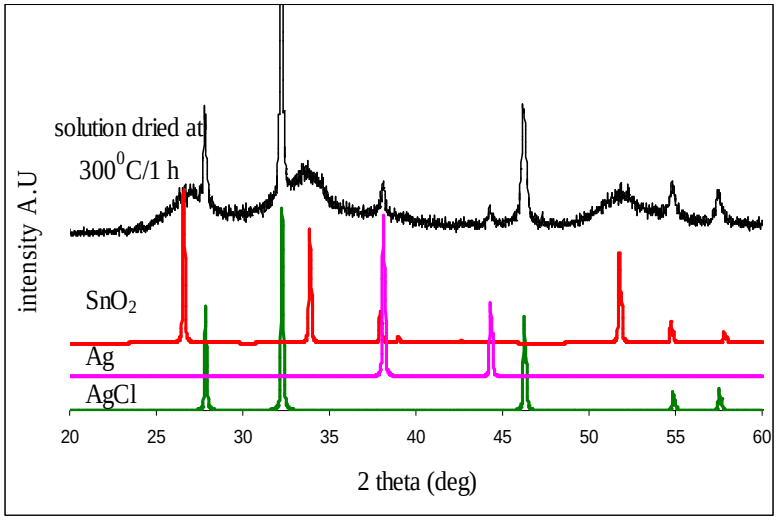

Figure 2.2 Powder X-ray diffraction peaks of Ag (s) added into spin coating solution which is dried at 300^0C for 1 h in air.

The reaction that occurs following addition of excess silver metal into the precursor solution can be written as:

$$Ag(s) + NO_3^-(aq) + 2H^+(aq) + Cl^-(aq) \longrightarrow AgCl(s) + NO_2(g) + H_2O(l) \qquad 2.4$$

It is seen in the reaction that the silver metal is oxidized to a 1+ oxidation state, while nitrogen is reduced from the 5+ oxidation state in the nitrate ion to the 4+ oxidation state in nitric oxide.

According to the electron microprobe analysis (EPMA) results (Table 2.1), the quantity of chlorine present in the films decreases significantly on heating. The chloride percentages are calculated relative to tin with the formula of 100x(Cl/Cl+Sn). Considering these results, it is seen that there is a considerable decrease in the chloride content following heating at temperatures as low as 200^0C. At 600^0C which is the temperature that TFT device performance is tested, the film has about 70.55 at % O, 0.03 at % Cl, 28.51 at % Sn and 0.91 at % Si. The Si content is largely associated with the substrate.

SnO_2	**% Cl (relative to Sn)**
as deposited	15.06
200 ^{0}C	0.21
600 ^{0}C	0.11
800 ^{0}C	0.07

Table 2.1 Cl content of tin (IV) oxide films as deposited and annealed for 1h in air.

Top and cross-sectional SEM images of films annealed in air at 600^0C for 1 h are shown in Figure 2.3. The film thickness is estimated to be 89 nm. It is seen that the

undoped SnO_2 films appear granular and rough, rather than homogenous and smooth, having small particle sizes of nanometer dimensions.

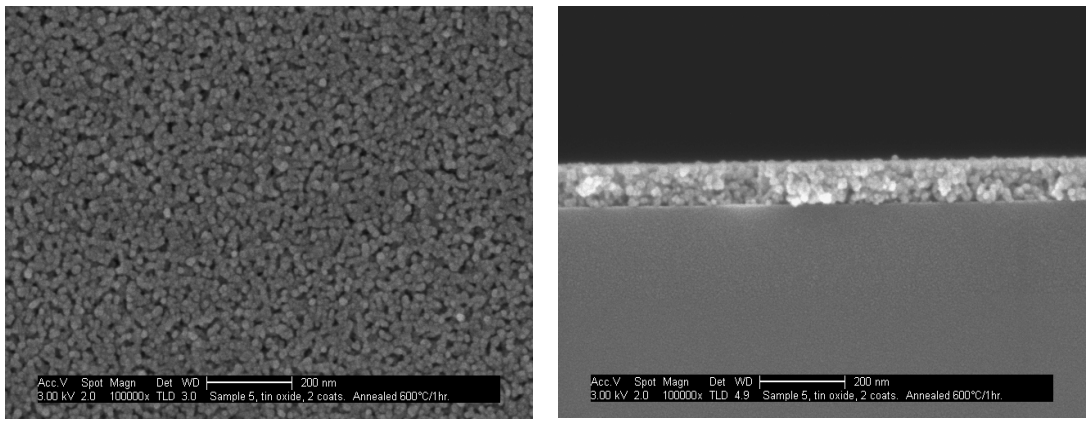

(a) (b)

Figure 2.3 (a) Top and (b) cross section views of Scanning Electron Microscope (SEM) images of the tin (IV) oxide film which is air annealed at 600^0C for 1 h.

IR measurements are performed to determine the decomposition temperature of the nitrate group and to monitor the removal of H_2O from the films. The measurements are done with the powders which are prepared from the dried spin coating solution at temperatures of 200, 300, 400 and 600^0C. According to the Figure 2.4 the nitrate absorption bands around 559, 677 and 1390 cm^{-1} dominantly seen at 200 and 300^0C however above 300^0C these strong absorption bands disappear. The absorption bands at 3500 cm^{-1} and 1665 cm^{-1} which are attributed to -OH stretch are strongly seen at temperatures 200^0C and 300^0C but mostly decreased above 400^0C. This is consistent with the thermogravimetric analysis (TGA) data of SnO_2 samples. Also it is proved that most of the hydroxyl group is gone up to 500^0C which is good because hydroxyls remain in the samples inhibit the growing of the SnO_2 crystallites (Toledo-Antonio, J.A., 2003).

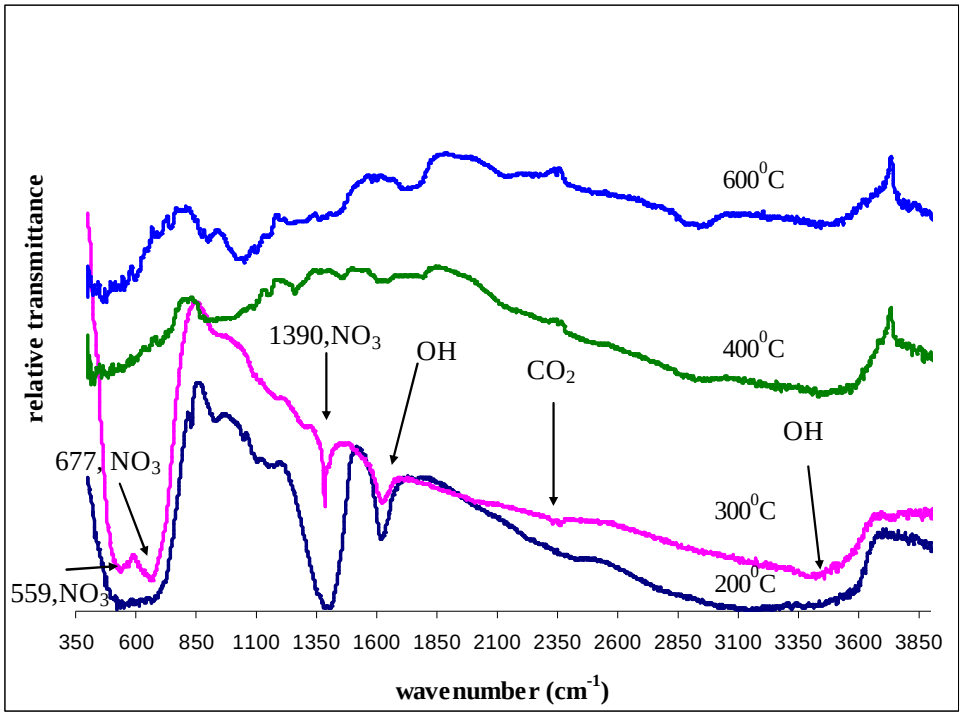

Figure 2.4 IR absorption data for tin oxide spin coating solution dried at temperatures of 200, 300, 400 and 600^{0}C.

Excess nitrate and chloride limit hydrolysis and generate stable [M(OH)(X)(OH$_2$)] (X=Cl or NO$_3$) complexes, affecting decomposition temperature. To eliminate the effects of chloride in the film a different reagent SnC_2O_4 is used to prepare the precursor solution. The reactions here are based on oxidation of Sn (II) to Sn (IV) by HNO_3 (aq) with additional solubility induced by coordination of the peroxo group.

In the spin-coating technique, gaseous products are given off on annealing the film. The occurrence of the tin (IV) oxide in the film is evident from the X-ray diffraction analysis shown in Figure 2.5. Here, the peaks from the as-deposited and air-annealed (600^{0}C) film are shown. The peaks match those from the silicon substrate and tin (IV) oxide. The peaks of tin (IV) oxide at 26.6, 33.9, 38.1 and 51.8^0 are evident in the film annealed at 600^{0}C. The films are annealed at 600^{0}C because, as demonstrated in the

literature, annealing tin (IV) oxide at 500^0C leaves only small amounts of residual hydroxyl groups in the film (Toledo-Antonio, J.A., 2003).

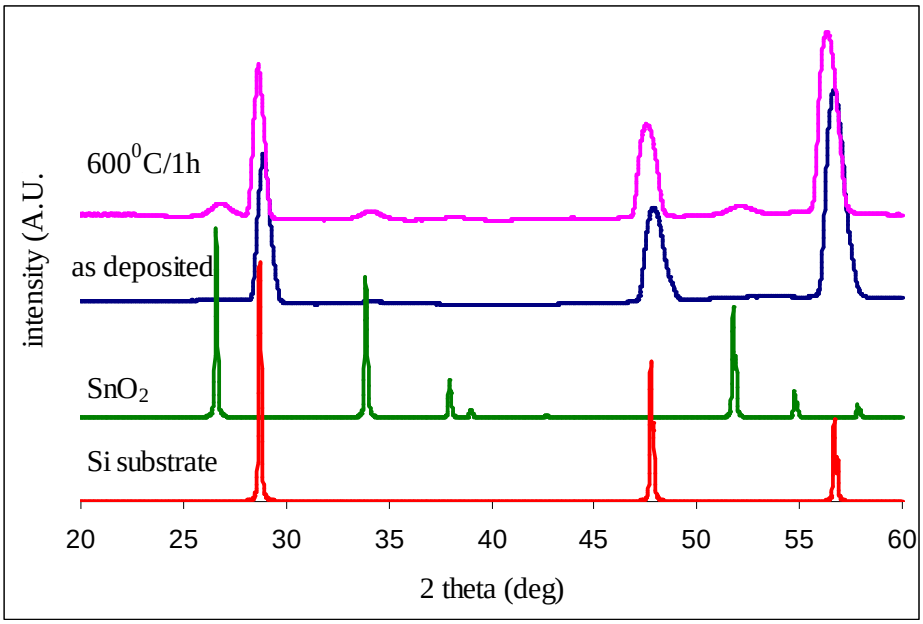

Figure 2.5 X-ray diffraction patterns for as-deposited and at 600^0C for 1 h annealed films.

Zinc-doped tin oxide films are deposited from a precursor produced by adding Zn metal to the hydroxo nitrato tin solution. The zinc metal dissolves according to reaction 2.5. As the Zn dissolves, the solution pH increases because of hydrogen ion consumption.

$$Sn^{4+}(aq)+OH^{-}(aq)+2NO_3^{-}(aq)+3Zn(s)+8H^{+}(aq) \longrightarrow Sn^{4+}(aq)+OH^{-}(aq)+2NO(g)+ 3Zn^{2+}(aq)+ 4H_2O(l) \quad 2.5$$

According to Table 2.2 the Zn concentration is approximately 10.5 at %; following an anneal at 800^0C, the concentration falls to 7.7 at %. The amount of chlorine

present in the films decreases significantly from 18.25 % in the as-deposited to 0.08 % in the film annealed for 1 h at 800^0C.

ZTO film	% Cl	% Zn
as deposited	18.25	10.47
200 ^{0}C	6.61	10.64
400 ^{0}C	0.89	9.75
600 ^{0}C	0.33	10.49
800 ^{0}C	0.08	7.74

Table 2.2 Electron Microprobe Analysis of zinc-doped tin oxide films as deposited and annealed at 200, 400, 600 and 800^0C for 1 h in air.

X-ray diffraction analysis of 10.5% Zn-doped tin oxide (ZTO) films annealed in air at 600 °C (Figure 2.6) indicates a significant rutile SnO_2 character with no zinc phases directly observed. SEM images for the 10.5 at % Zn-doped SnO_2 film annealed at 600^0C are shown in Figure 2.7. In comparison to those of undoped SnO_2 (Figure 2.3), smaller grain sizes, a higher density, and smoother surface may be noted.

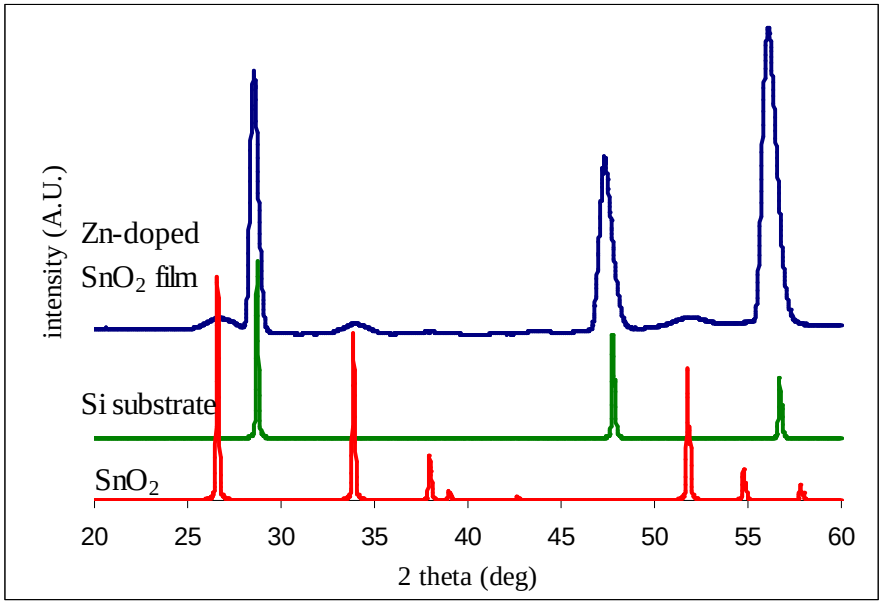

Figure 2.6 X-ray thin film data of ZTO film annealed at 600^0C/1h in air with the matching peaks of Si (substrate) and SnO_2

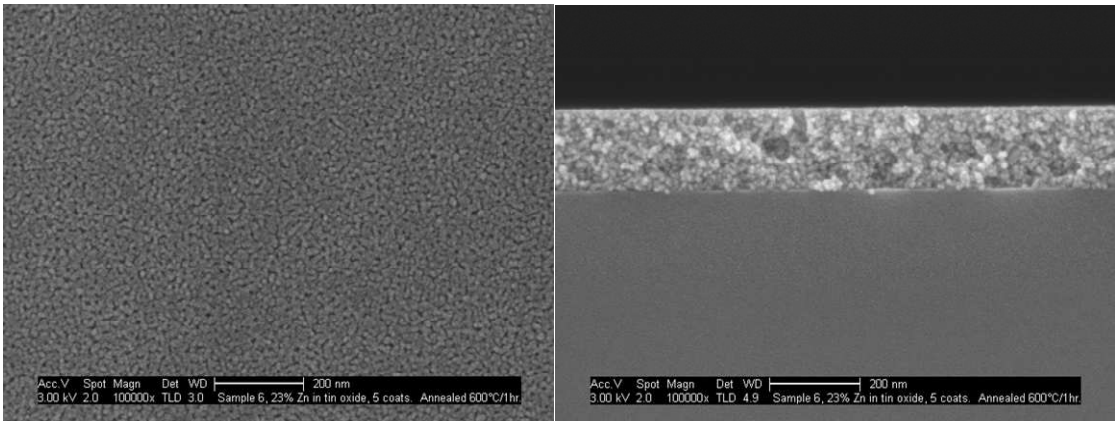

(a) (b)

Figure 2.7 (a) Top and (b) cross-section SEM images of the 10.5% Zn-doped tin oxide films, which are annealed at 600^0C for 1 h.

Since it is demonstrated (Srinivasa M.N., et al, 1983) that doping with electronic donor such as Sb^{5+} decreases resistivity initially up to about 3 mol % goes through a minimum and then increases again for higher antimony concentrations. The 3.18 % (evident form EPMA analysis) antimony doping into tin (IV) oxide is performed to obtain a conductor. The reactions of antimony metal addition are shown in reaction 2.7.

$$Sn^{4+}(aq) + Sb(s) + NH_3(aq) + H_2O \longrightarrow \text{antimony tin hydroxide gel} \qquad 2.7$$

After centrifuge and wash steps with EtOH and H_2O mixture the washed gel is dissolved in HNO_3 (aq) to obtain a clear spin coating solution. The mol ratio of Sn to HNO_3 is 1.73 to 1 and the total metal (Sb+Sn) to HNO_3 is 1.82:1. Spin coating this solution turned to Sb-doped tin oxide films. It is evident form Figure 2.8 that SnO_2 phase is crystallized at 600^0C compared to the as deposited film data. The antimony atom is not seen in X-ray diffraction analyses in Figure 2.8 however it is detected from EPMA analysis. The EPMA showed that at 600^0C the atomic mol ratios are 63.25% O, 0.36% Cl, 11.22% Si, 24.36% Sn and 0.80% Sb. The percentage of antimony relative to tin [100 x (Sb/Sb+Sn)] is calculated to be 3.18%.

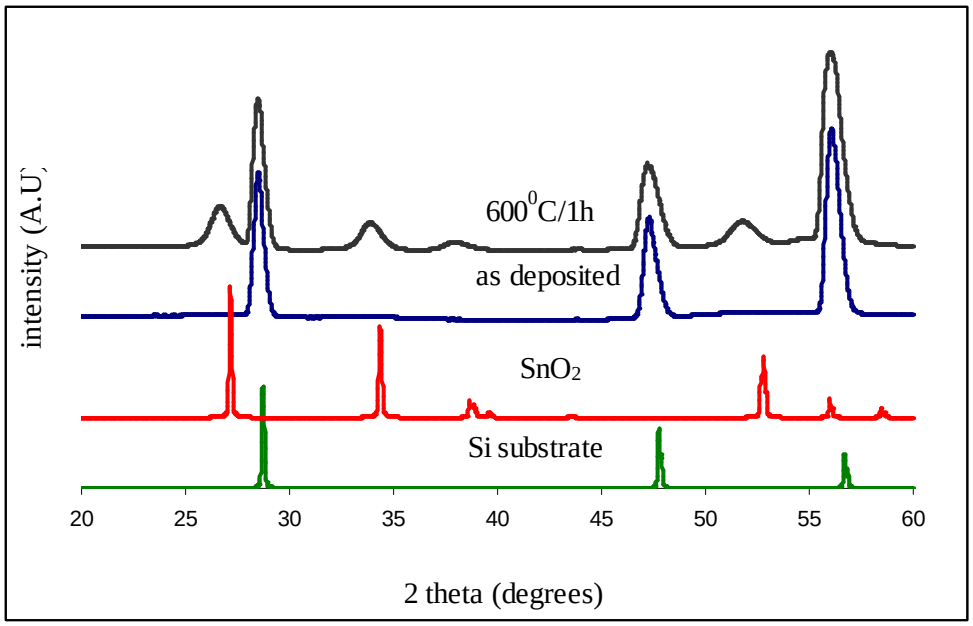

Figure 2.8 X-ray data of 92 nm thick, 3.18% Sb doped SnO_2 film as deposited and air annealed at 600^0C for 1 h.

The SEM images of the 3.18% Sb doped SnO_2 films are shown in Figure 2.9. The film looks granular and has small particle size but a smooth surface is evident from the cross section image. (Figure 2.9-b)

Antimony doped SnO_2 showed a resistivity of 34 mohm cm for a film of ~75 nm thickness which is air annealed at 600^0C for 1 h. Compared to the resistivity (5-6 ohm cm) for a film of ~40 nm thickness which is air annealed at 600^0C for 1 h measured for undoped tin (IV) oxide films a decrease in the resistivity observed for antimony doped ones (thicknesses are estimated from SEM).

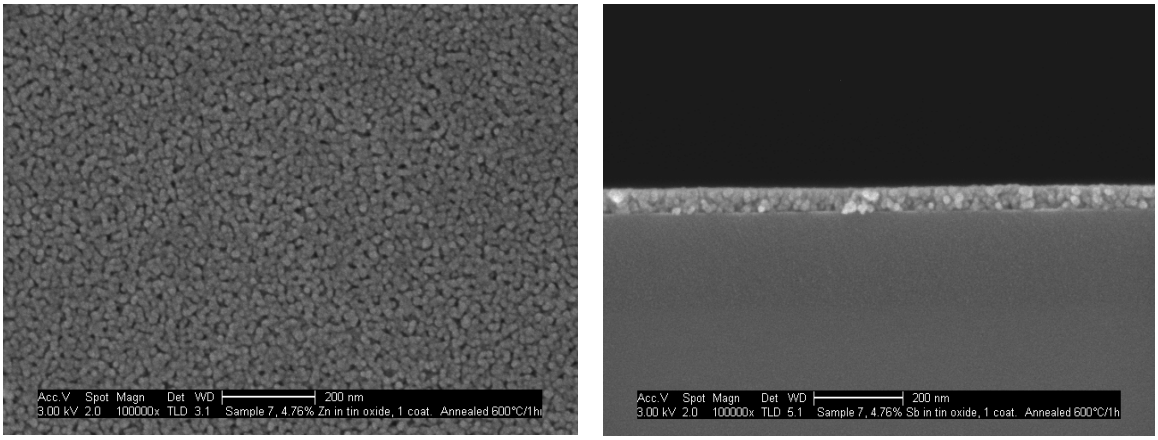

Figure 2.9 Top (left) and cross section (right) views of SEM images of 46-nm thick 3.18 at % Sb-doped tin oxide films.

Electrical Characterization

Spin-coated, 40 nm thick SnO_2 films annealed at 600°C for 1 h exhibit a resistivity of 5-6 ohm cm. 10.5 % Zn-doped SnO_2 films annealed at the same temperature demonstrate ~500 Mohm cm resistivity, so they are insulating. TFTs are prepared on heavily doped p-type silicon substrates with 100 nm of thermal silicon dioxide gate dielectric layer formed via thermal oxidation and a tantalum/gold back contact. A channel layer of 45-nm thick tin oxide layer is then deposited via spin coating (Figure 2.10).

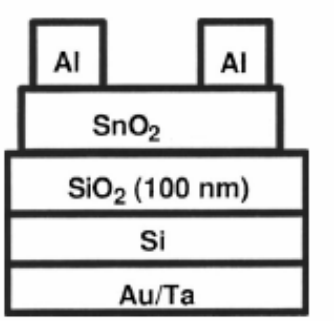

Figure 2.10 Cross sectional view of the bottom gate TFT device with undoped SnO_2 channel layer

Bottom-gate TFTs fabricated from pure SnO_2 films could not be characterized because of high channel conductivity. The SEM images of the films are seen in Figure 2.3. From this image the granular nature of the film is realized. In undoped-SnO_2 there are approximately 40-nm diameter sphere like particles with vacancies between them which may cause the film to have many defects. So, the lack of densification of the film or being a too conductive channel layer can make it hard to behave as a transistor. This behavior of the SnO_2 films are consistent with the results of Presley et al. Their films are deposited by RF magnetron sputtering and then rapid thermal annealed in O_2 at 600^0C. They stated that the reason of being too conductive for an annealed SnO_2 thin film is the tendency of SnO_2 to form oxygen vacancies, which provide extra electrons to the conduction-band (Hartnagel H.L., et al, 1995). If the channel layer conductivity is too high, it can not be modulated by a gate voltage, which makes the transistor operation impossible. However the transistor behavior is possible if the channel-layer conductivity is decreased to a certain level. They propose that it is possible to minimize the channel-layer conductivity by decreasing the channel-layer thickness to ~10-20 nm which helps to reduce the conductivity of the SnO_2 films (Presley R.E., et al, 2004).

The zinc doped tin oxide bottom gate TFT layout is the same as tin oxide TFT device except for the channel material. The ZTO channel layer thickness is approximately 40 nm.

The bottom-gate TFT fabricated from ZTO film exhibits a reduced channel conductivity with respect to the TFT fabricated from pure SnO_2 film. Looking at the grain morphology in the SEM images of ZTO films in Figure 2.7, it will be noticed that there are isolated grains forming grain boundary scattering which possibly reduce the mobility of the ZTO device. The grain boundary scattering is not surprising if the polycrystalline nature of the ZTO films is considered. The morphology of the ZTO films makes it evident that the films have dehydrated particles rather than hydrated ones and having dehydrated particles and being nondense in nature most possibly decreases the hydroxo polymerization. As a result the device behavior is attributed to many things like poor grain morphology, possible retention of chloride counterion and the small amount of Zn doping that the SnO_2 film contains which leads to high concentration of electron traps that leads to the inability to turn the device on. The film likely to contain Zn:SnO_2 and ZnO. However ZnO is not seen in the X-ray patterns shown here, as its concentration is too low.

Solution Deposition of Cuprous Oxide Thin Films

Chapter 3

Abstract

The deposition of cuprous oxide thin films from aqueous solutions of copper (II) formate tetrahydrate is achieved by spin coating with post annealing under a nitrogen atmosphere at temperatures $\leq 400^0$C. Morphologies of these thermally treated films are compared to those produced via photoexposure with wavelengths in the range 254 to 436 nm.

X-ray diffraction, atomic force microscopy (AFM) and scanning electron microscopy (SEM) are used to characterize the films. UV spectrometer is used to identify the UV absorption wavelength of copper (II) formate tetrahydrate.

Introduction

Cu_2O is known as a p-type semiconductor, and its potential application in solar cells has attracted much attention because of its low cost, high solar absorbance, low thermal emittance, nontoxicity, and simple process of manufacture (Luzeau P., et al, 1990). The p-type nature of Cu_2O is derives from the positive holes associated with ionized copper vacancies and interstitial oxygen atoms (Porat O., et al, 1995). The band gap of Cu_2O is 2.17 eV, and a single crystal mobility of 40 $cm^2 V^{-1} s^{-1}$ has been reported (Buljan A., 2001). Cu_2O has a wider energy gap compared with cupric oxide, which is around 2.0 eV (Portier J., et al, 2004).

For the preparation of the polycrystalline thin and thick films of cuprous oxide there are many techniques such as thermal and chemical oxidation of copper, electrodeposition, and reactive sputtering, as reviewed by Rakhshani A. E., 1986 and Rai B.P., 1988 for their use in solar cells. The depositions on glass substrates are usually applied by techniques such as reactive sputtering (Beensh-Marchwicka G., 1982) and vacuum evaporation (Pankov Ju. D., 1978). The chemical deposition of a Cu_2O film on a glass substrate was first reported by Ristov M., et al, 1985. Ristov's method consists of alternate immersions of a substrate in a solution of NaOH at temperatures between 50^0C and 90^0C and in a solution containing a copper complex (25^0C) repeated over several cycles. This technique was modified by Nair M.T.S., et al by eliminating the rinsing step between the immersion cycles to deposit a Cu_2O film onto a microscope glass slide in 1999.

According to Nair M.T.S, et al's results annealing the deposited film in air at 300^0C led to a partial conversion of Cu_2O to CuO, and annealing at 350^0C led to a total conversion of the material to CuO. As the reaction proceeded the colorless solution changed to yellow–orange and brown-black due to the formation of Cu_2O and CuO respectively. On the other hand, the crystallinity of the films and the composition of Cu_2O remained unchanged during the annealing under nitrogen gas at temperatures of up to 400^0C. The conversion of Cu_2O to CuO during heating in the presence of oxygen is known (Trotman-Dickenson A.F., 1973). In the bulk form the conversion is reported to take place at temperatures above 400^0C. It is also reported that at still higher temperature, CuO could change to Cu_2O.

The electrical conductivity of a 0.15 µm thick Cu_2O film is reported about $5x10^{-4}$ $\Omega^{-1}cm^{-1}$. The electrical conductivity of this film increased about an order of magnitude ($5x10^{-3}$ $\Omega^{-1}cm^{-1}$) when the film was annealed in nitrogen at 400^0C. The increase in conductivity with annealing temperature under air was also reported. The dark conductivity of the CuO film produced by air annealing of a 0.15 µm Cu_2O film at 400^0C is about $7x10^{-3}$ $\Omega^{-1}cm^{-1}$ (Nair M.T.S, et al, 1999).

The crystal structure of Cu_2O is known to be in cuprite structure as shown in Figure 3.1. It is formed by bcc array of oxygen atoms with copper atoms between two consecutive oxygen layers. Copper forms linear O-Cu-O bonds with oxygen where oxygen atoms are surrounded by a tetrahedron of copper atoms. As seen from the Figure 3.1 each copper atom is two-coordinated and each oxygen atom is four coordinated.

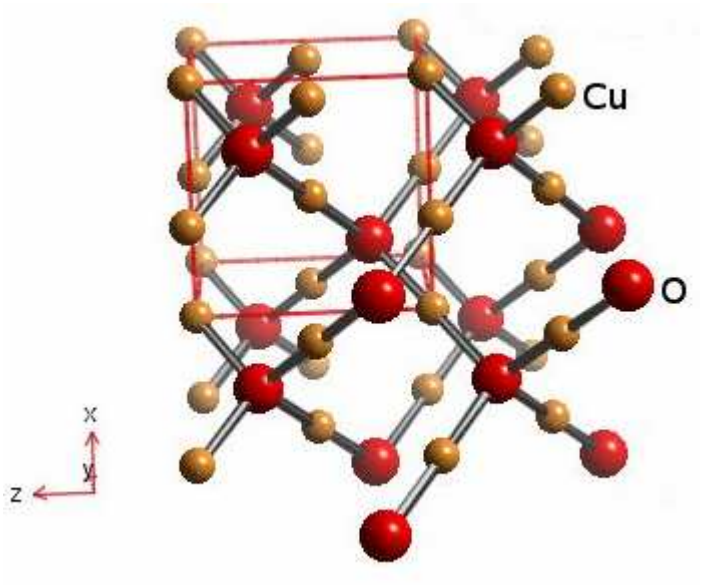

Figure 3.1 Crystal structure of Cu_2O where large spheres represent O and small spheres represent Cu.

It is known that the salts of carboxylic acids and especially formates decompose in oxidant-free media to give metals. The decomposition of these salts is exothermic and occurs with a high rate at relatively low temperatures. According to derivative thermogravimetric (DTG) curve of anhydrous copper (II) formate the decomposition occurs at one stage at a temperature of 180^0C and the resulting metallic copper is oxidized to Cu_2O (220^0C) and later to CuO (355^0C) (Efremov et al, 2002).

In this study, aqueous solutions of copper formate tetrahydrate are chosen as precursors for the deposition of cuprous oxide films. According to Mohamed and co-workers, decomposition in air of anhydrous copper (II) formate to copper (I) formate then copper metal is claimed to be complete at approximately 238^0C together with two exothermic peaks observed at 184^0C and 219^0C evident from differential thermal analysis (DTA). These exothermic peaks are confirmed by derivative thermogravimetric (DTG) analysis that they correspond to the peaks observed at around 175^0C and 224^0C which attributed to the mass losses of total 52.3 %, evidence of significant oxide product formation. The continued mass increase after decomposition was related to the slow oxidation of metallic Cu or Cu_2O present in the residual products at 245^0C (Mohamed M.A., et al., 2004). According to Narsimlu and co-workers, the optical absorption spectrum of α-Cu $(HCOO)_2$ single crystal exhibits one absorption band in the UV region at 28571 cm^{-1} and another band in the visible region at 14285 cm^{-1}. The absorption band occurring at 28571 cm^{-1} is attributed to a charge transfer from the ligand formate ion - $COOH^{-1}$ to the central Cu (II) metal ion. The broad peak occurring at 14285 cm^{-1} has been ascribed to the ligand-field splitting of the $3d^9$ energy levels of the copper (II) ion (Narsimlu et al., 1996).

In the process of solution deposition, polymerization in the precursor solution is quite important for the purpose of obtaining a continuous film. Polymerization can be formed by condensation reactions involving either hydroxylation or oxolation. In some cases, polymerization and condensation can be induced via optical excitation and decomposition of an organic moiety such as formate. Ultraviolet light (λ~ 348 nm) has been previously used to decompose copper (II) formate. Cu (II) is initially reduced to Cu (I) and then later reduced to Cu (0) (Vigil E., et al, 2005). From this perspective it is thought to decompose the precursor copper (II) formate and cure the resulting cuprous oxide films by UV light. Hence, photo-induced decomposition of copper (II) formate provides a potential route to the production of Cu_2O films.

Experimental

Cuprous oxide (Cu_2O) films were prepared from aqueous solutions of 0.4 M $Cu(HCOO)_2.4H_2O$ (98%, Alfa Aesar) by spin coating annealing under nitrogen atmosphere at temperatures $\leq 400^0$C.

The substrate used for the deposition was silicon with a 1700 Å thick coating of SiO_2. Substrates are cleaned at 45^0C for 60 min in an ultrasonic bath containing Conrad 70 detergent. Prior to use the substrates are washed with millipore water and dried under a stream of N_2 (g). Spin coating this solution at a rate of 3000 rpm for 30 s resulted in colored films. The copper formate solution was cast onto the substrate with annealing at 120^0C for 1 min between each coat.

The UV photoexposure to the films is performed by various UV sources. After the first layer of the film is spin coated the film is exposed to UV light for ~30 min period then the next layer of the film is spin-coated. This procedure is followed 8 times until the desired film thickness is obtained. The experiment with the hand lamp (model UVG-54) was performed by setting it in a nitrogen glove box. The film is spin coated and exposed to UV light between each consecutive coat in the nitrogen glove box for 15 min. The company named Optical Associates, Inc. (OAI) in California analyzed the films with a UV source having a wavelength of 260 nm. Their exposed power density and the exposure time were 18.3 mW/cm^2 and 30 min respectively. A thermocouple is attached to the bottom of each sample and the temperatures are measured in the beginning and at the end of the process which occurred between 71^0C and 78^0C.

UV photoexposure was achieved by using an RPR-100 UV reactor (12 mercury lamps with 254-nm output providing a power of 35 watts and a power density of ~ 0.0128 W/cm^2) or a UVG-54 hand-held lamp (254-nm output providing a power of 6 W). The other UV sources used are Hg short arc HAS-200 lamp provided by Advanced Radiation Corporation Company (300 to 436 nm output providing a power of 200 W and a power density of 0.018 W/cm^2) and a UV lamp provided by Optical Associates, Inc.

(OAI) (260 nm output providing a power density of 0.018 W/cm^2). The RPR-100 UV reactor and UVG-54 hand lamp are found in our laboratory.

Thin-film X-ray data were collected with a Rigaku/MSC Rapid diffractometer, employing Cu Kα radiation generated from a rotating anode at 50 kV and 270 mA. A Siemens (Bruker) D5000 diffractometer was used to collect powder X-ray data (Cu radiation), atomic force microscopy (AFM) is used for the identification of the surface morphologies and scanning electron microscopy (SEM) data were acquired at Hewlett Packard.

Results and Discussion

As previously mentioned on heating copper formate tetrahydrate organic decomposition is completed at around 238^{0}C (Mohamed M.A., et al, 2004), where carbon dioxide and hydrogen are evolved. The suggested mechanism for the decomposition is written as in reaction 3.1. In this reaction Cu (II) is reduced to Cu (0) with an intermediate product of copper (I) formate (Galwey A.K., et al, 1974).

$$Cu(HCO_2)_2 \longrightarrow Cu + 2CO_2 + H_2 \qquad 3.1$$

According to Mohamed M.A., et al, from thermogravimetric analysis under nitrogen atmosphere a mass loss is observed up to 213^{0}C with Cu metal formation and then above 215^{0}C there occurred a slow mass increase which attributed to Cu_2O and CuO formation. They concluded this result as the traces of oxygen found in N_2 gas environment. According to their results, copper metal is the primary solid product for the decomposition of copper (II) formate under an inert atmosphere. In air, after the

decomposition of anhydrous copper (II) formate a slow oxidation of metallic Cu or residual Cu_2O is observed. Under a hydrogen atmosphere, annealing resulted in only Cu metal (Mohamed M.A., et al, 2004).

In the process of spin coating the copper (II) formate tetra hydrate precursor, the solid product formed on the films following an anneal in a nitrogen atmosphere is confirmed by X-ray diffraction as cuprous oxide (Figure 3.2). The X-ray diffraction peaks of the annealed film at 400^0C for 2h 30 min under nitrogen atmosphere, the air annealed film at 300^0C for 2h are compared with the reference peaks of Cu metal, Cu_2O, CuO and the Si substrate.

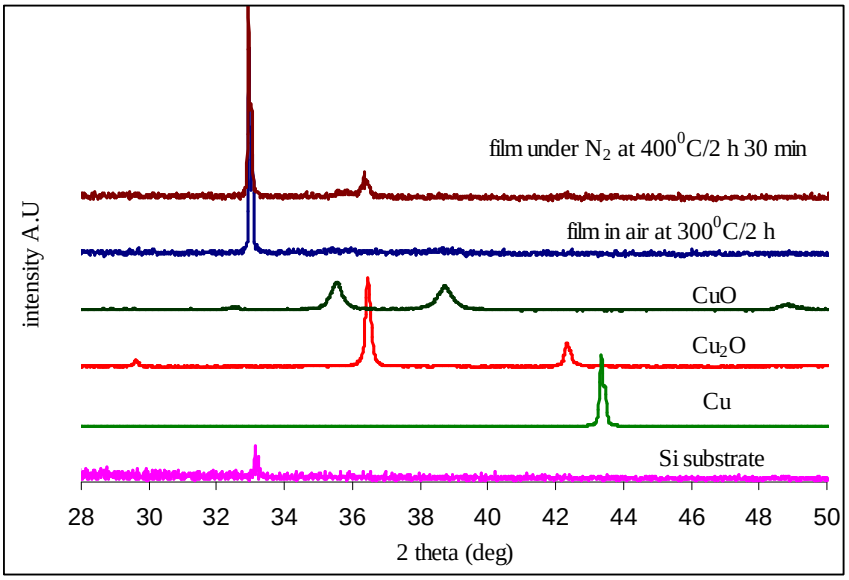

Figure 3.2 X-ray data of the thin film annealed at 400^0C for 2 h and 30 min under N_2 atmosphere and thin film annealed at 300^0C for 2 h in air.

For the film annealed at 400^0C for 2 h 30 min under nitrogen atmosphere there are matching peaks of the Si/SiO_2 substrate at 32.6^0 of 2θ, cuprous oxide at around 36.4^0 of 2θ and 42.3^0 of 2θ, however the peaks of the air annealed film at 300^0C for 2h only

matched with the substrate peak. It is noticed from Figure 3.2 that the diffraction peaks of the film annealed under nitrogen atmosphere do not match with the peaks of CuO and Cu metal.

The obtained Cu_2O film by annealing under N_2 (g) atmosphere which is confirmed by X-ray data can be the result of oxidation of the films. The films are annealed for a long time (2 h 30 min) under nitrogen environment that it is possible to have some residual oxygen in the N_2 (g).

Instead of the thermal treatment applied under nitrogen atmosphere after the deposition of the films, UV light is used to decompose the as-deposited film. The evidence of the UV light shined film being in cuprous oxide structure is shown by the X-ray data in Figure 3.3. It will be noticed from the figure that the other possible copper phases of copper metal and cupric oxide peaks did not match with the obtained data of the film itself.

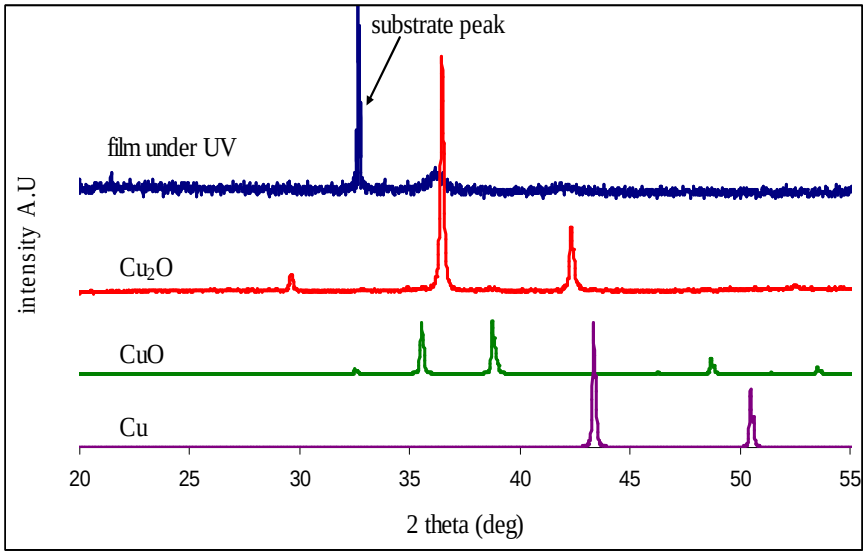

Figure 3.3 X-ray data of the thin film spin coated and exposed to UV light

The morphologies of the deposited films are obtained by the atomic force microscope analysis. In Figure 3.4 the AFM image of the cuprous oxide film which is thermally annealed between coats at 120^0C on hot plate followed by post-annealing at 300^0C for 2 h in air is shown. In order to cure the film the last step applied as a UV treatment for 45 min with a UV reactor giving of a wavelength of 254 nm. The RMS roughness is around 35 nm for this film.

In Figure 3.5 the cuprous oxide film which is decomposed with UV light between each coat for about 15 min is seen. The film has a RMS roughness of 4.47 nm and a thickness of about 78 nm which is estimated from the SEM results. As a comparison between the thermally treated followed by UV shined and only UV decomposed films there is a difference in roughness where in the latter less rough films are obtained. Considering the morphologies of both films it is seen from the AFM images that the film that has been only UV shined possesses a smoother surface and smaller grains. But still images show that the two films are granular which is not so preferable in the use of a channel layer of a TFT device.

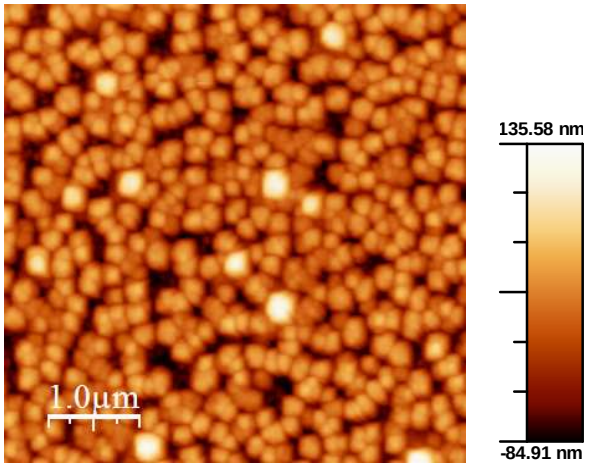

Figure 3.4 The cuprous oxide film which is annealed at 300^0C for 2 h in air following an exposure to UV light of 253.7 nm for 45 min. RMS roughness of the film is 35 nm.

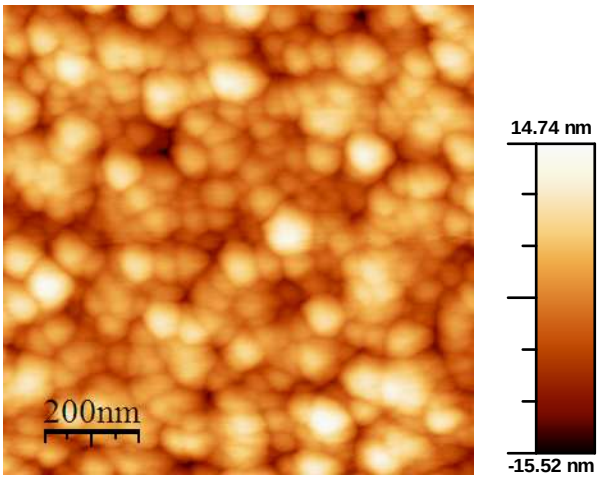

Figure 3.5 The cuprous oxide film which is exposed to UV light between coats for ~15 min with a RMS roughness of 4.47 nm and a thickness of ~78 nm.

In order to see the morphologies of the films from other perspectives SEM analyses are done. The SEM images of the UV decomposed cuprous oxide films are shown in Figure 3.6. Between the coats 253.7 nm wavelength of UV light was shined on them for 30 min with RPR-100 UV reactor. The temperature inside the reactor is measured to be 35^0C.

From the Figure 3.6 (b) it can be noticed that the film is granular but the surface of the film is smooth and from Figure 3.6 (c) the thickness of the films can be measured as approximately 78 nm for eight coats.

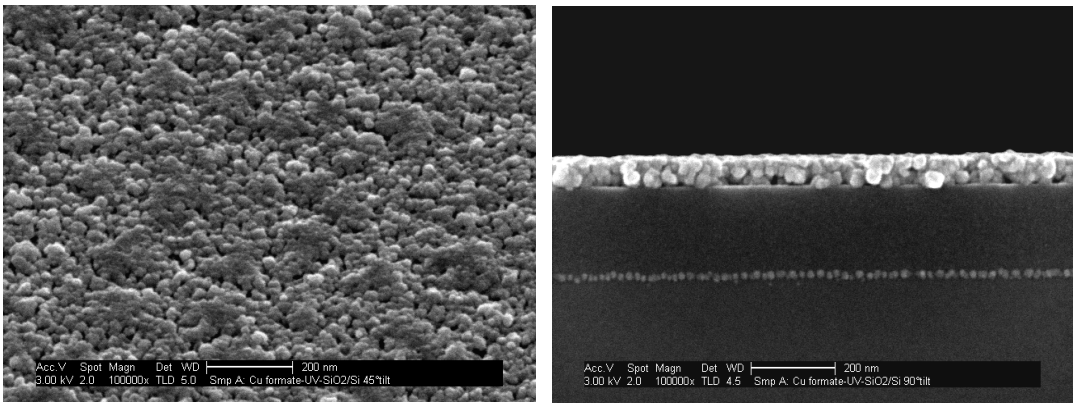

(a) (b)

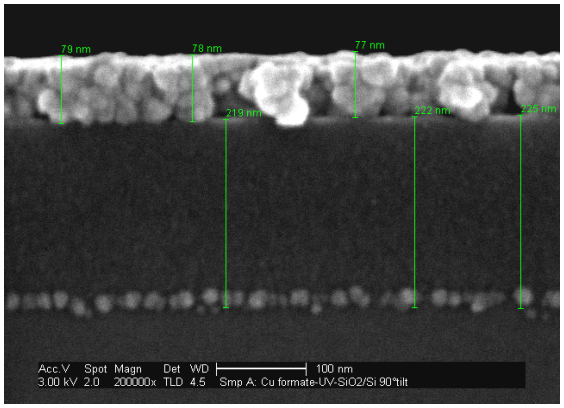

(c)

Figure 3.6 The SEM of (a) top view, (b) cross section view in 200 nm scale, (c) cross section view in 100 nm scale of cuprous oxide film whose surface is decomposed via UV light for 30 min for each coat.

In Figure 3.7 the SEM image of a film is shown which is decomposed via UV light followed by a N_2 atmosphere anneal at 300^0C for 1 h 45 min. As it is expected annealing under nitrogen atmosphere at 300^0C turned the film into crystalline cuprous oxide phase confirmed by X-ray diffraction analysis.

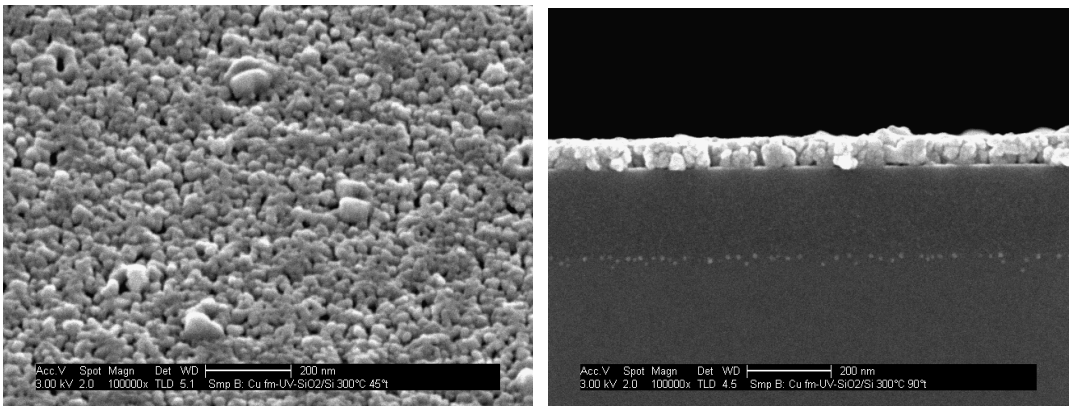

(a) (b)

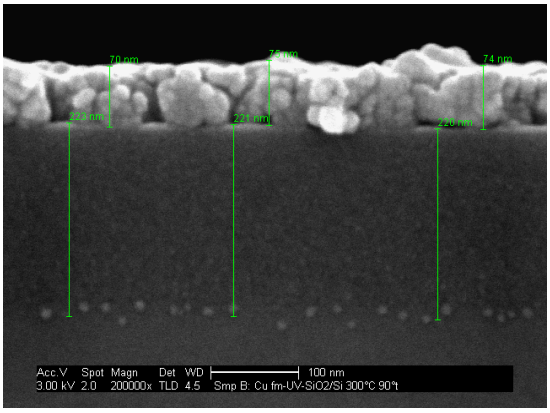

(c)

Figure 3.7 The SEM of (a) top view, (b) cross section view in 200 nm scale, (c) cross section view in 100 nm scale of cuprous oxide film whose surface is decomposed via UV light following an anneal under N_2 atmosphere at 300^0C for 1:45 hour.

As a comparison of the SEM images shown in Figure 3.6 and Figure 3.7 only UV decomposition or UV decomposition followed by an anneal under nitrogen atmosphere creates no big difference in morphology. However in Figure 3.7 a rougher film which contains bigger particles is realized which can be attributed to the crystallization achieved

by the thermal anneal. In the exposition of these films the UV reactor used had a wavelength of only 254 nm which is not the exact UV absorption wavelength of the precursor of copper (II) formate tetrahydrate.

According to the literature the UV absorption band of α-Cu $(COOH)_2$ single crystal shows one absorption band in the UV region at 350 nm (Narsimlu N., et al, 1996). So to learn the absorption wavelength of the copper (II) formate tetrahydrate, the aqueous solutions of copper (II) formate tetrahydrate in the concentrations of 0.4 M, 4.10^{-3} M and 4.10^{-4} M are prepared and analyzed with a spectrometer which is in the range of wavelengths between 200 nm and 800 nm. According to the spectrogram shown in Figure 3.8 the absorption of copper (II) formate tetrahydrate in the UV region is seen at below 350 nm and the second absorption is seen in the visible region starting from 550 nm for the 0.4 M of solution and 650 nm for the more diluted ones. Since it is shown that copper (II) formate tetrahydrate absorbs light below 350 nm in the UV region it is preferable to have a UV source that will give a wavelength below 350 nm. So, for the exposition of the films the UV source was chosen in the wavelength of 254 nm.

Since it is confirmed that UV light can decompose the films into cuprous oxide as well as nitrogen annealing the other way tried was shining the UV light under nitrogen atmosphere. In the films that are obtained from the UV source in nitrogen glove box, it was not observed any noticeable thickness building. For this reason looking for a more powerful source (more than 6 Watts total) and a broad wavelength spectrum (below 350 nm) was necessary. So, the films have been sent to two different companies in the name of Advanced Radiation Corporation (ARC) and Optical Associates, Inc. (OAI) to be analyzed with UV sources of different wavelengths.

By comparing the morphology of the films exposed to UV light by the OAI Company and the ones exposed to UV light provided by RPR-100 UV reactor (Figure 3.5) not much difference is observed

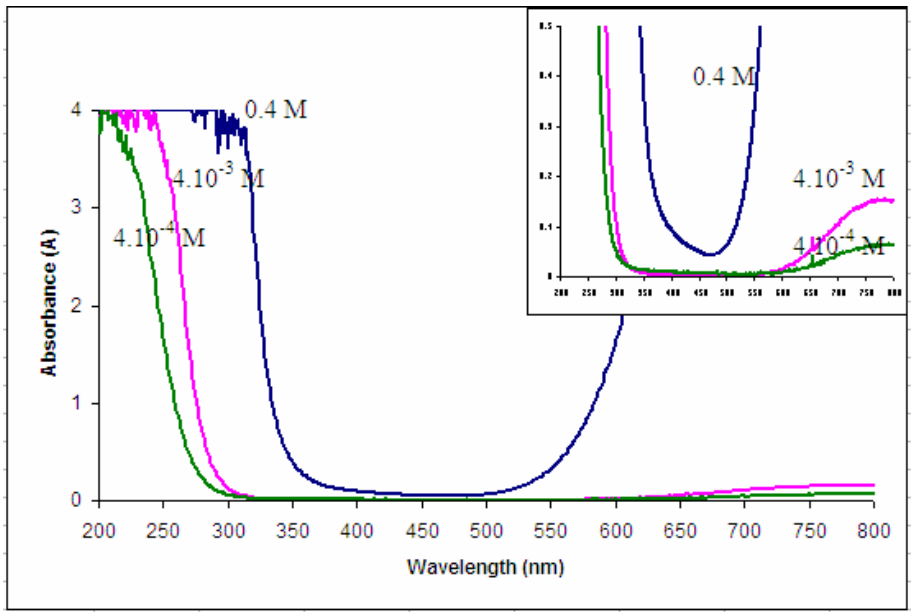

Figure 3.8 The absorption spectrum of copper (II) formate tetrahydrate solutions in the concentrations of 0.4 M, 4.10^{-3} M and 4.10^{-4} M between wavelengths of 200 nm and 800 nm.

This is also evident from the Figures 3.9 and 3.10. In the Figure 3.5 the film which is UV exposed by a RPR-100 UV reactor between the consecutive coats for 15 min showed a roughness of 4.47 nm on the other hand the films exposed to UV light by OAI Company showed a roughness of 2.3 nm and 3.95 nm evident from the Figures 3.9 and 3.10 respectively. The film seen in Figure 3.9 is approximately 9.75 nm thick which is once coated and exposed to a UV light for 30 min. The film seen in Figure 3.10 is approximately 78 nm thick which is exposed to UV light with the RPR-100 UV reactor for 30 min between each coat and the post-anneal is performed by the OAI Company with the same UV source for the same amount of time. These results can be evaluated by looking at the roughness values of the films in terms of morphology. The least rough films are obtained by both UV shining between the coats following a post anneal with UV. This film morphology can be seen in Figure 3.10.

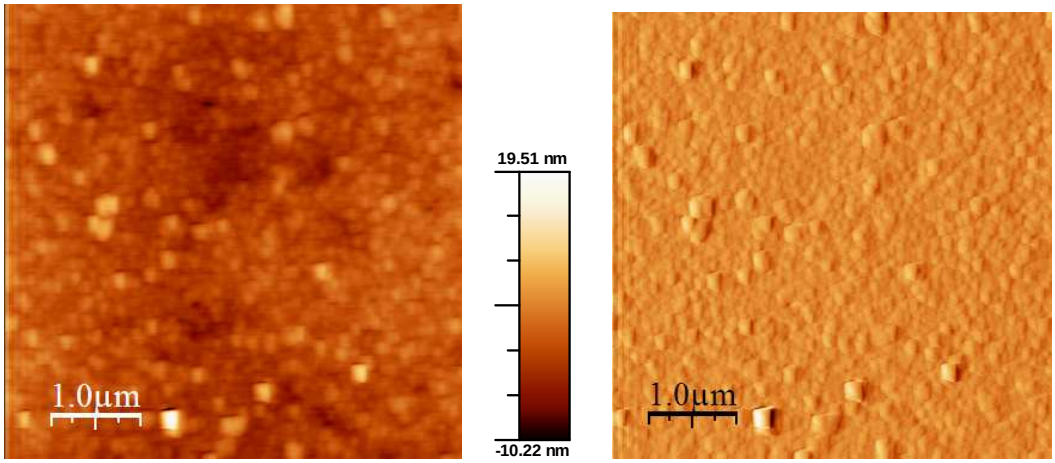

(a) (b)

Figure 3.9 (a) AFM image of the ~9.75 nm thick cuprous oxide film exposed to UV light by OAI. The film has a surface roughness of 2.3 nm (b) deflection image of the same film.

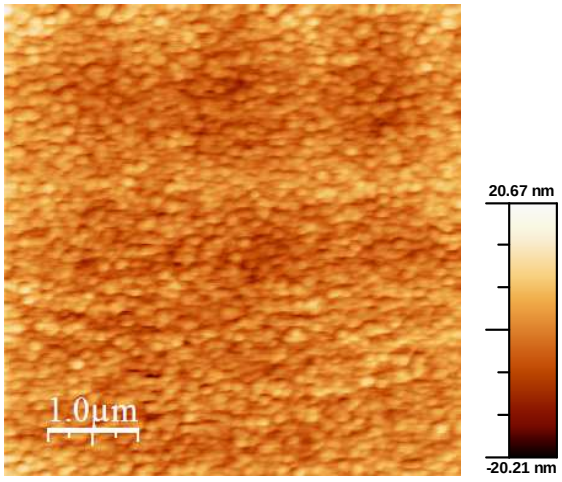

Figure 3.10 AFM image of the ~78 nm thick cuprous oxide film exposed by RPR-100 UV reactor and exposed to UV by OAI. The film shows a surface roughness of 3.95 nm.

Solution Deposition of Silver Metal Thin Films

Chapter 4

Abstract

Conductive materials have many application areas such as electrodes, pixel pads, conductive lines, and tracks in enabling low-cost electronics (Li Y., et al, 2005). The conductors prepared from organic materials are poor in conductivity and long term stability. For the purpose of direct ink deposition of metals the most common approach is the deposition of nanoparticles (Stathatos E., et al, 2000). However there are some limitations of this type of deposition such as high annealing temperatures and inferior mechanical properties. The gold and silver nanoparticles are the primary candidates that show promising conductivities (~10^4-10^5 S cm^{-1}) at high temperature and vacuum conditions. The high cost of gold makes it non preferable over silver particles and the high temperatures (> 300^0C) which are not suitable for flexible plastic substrates lead to looking for new deposition routes.

The solution deposition of silver metal at low temperatures is the primary goal of this work. Our approach is the deposition of the silver metal films directly from solution with the method of spin coating. A solution of silver (I) oxide dissolved in concentrated aqueous ammonia is used as the precursor; silver metal is directly realized with curing temperatures as low as 120^0C.

The deposited silver films are confirmed via X-ray diffraction, and the morphology of the films is characterized by atomic force microscopy (AFM) measurements.

Introduction

Silver metal is widely used as an IR reflective material in low-emissivity coatings and solar control layer stacks in automative windows (Sahm H. et al, 2004). Silver thin layer is usually covered with protective dielectric layers like ITO and pure In_2O_3 due to its poor atmospheric stability (Ando E., et al, 2001). Other applications of the silver are in soldering alloys, high-capacity batteries, electrical equipment, and printed circuits. The silver salts are also extensively employed in the photographic industry (Housecroft C.E., et al, 2001).

Solution deposition and printing of the metal films has traditionally been centered on the use of micron-sized flakes and nanoparticles. By printing and annealing nanoparticulate suspensions of gold, silver, and other metals it is possible to form conductors for electronics applications. Such sintered materials however have exhibited poor mechanical properties and relatively high porosity

Liquid-based deposition and patterning of transistor circuits are being studied as a low-cost alternative to amorphous silicon technologies for electronics. These circuits have many applications such as large-area electronics (e.g., active-matrix LCDs, organic light emitting diodes, e-paper) and low-end devices (e.g., wearable electronics, smart labels, radio frequency identification tags), where mechanical flexibility is required. Liquid processable semiconductors for channel layers are mostly investigated for printed electronics however there is not too much research done in printable conductive materials. Some of the applications areas of conductive materials are electrodes, pixel pads, conductive lines, and tracks in enabling low-cost electronics (Li Y., et al, 2005).

Earlier printable conductor works focused on organic materials, which exhibit low electrical conductivity (< 3 S cm^{-1}) and their poor chemical, thermal, and electrical stabilities. Gold and silver metals exhibit high conductivity (~10^4-10^5 Scm^{-1}) and operational stability, but high temperature and high vacuum conditions are necessary for their deposition. Gold nanoparticles have been deposited by Wu Y., et al in 2005 with a low-temperature method however its high cost does not make it a preferable material. For this reason, low-cost, solution-processed silver materials are preferred if a deposition

method is found which provides its high conductivity and low-temperature requirements together (Li Y., et al, 2005).

Commercial silver pastes and inks have a low thin film conductivity (Gray C., et al, 2001) which is around 2000 S cm^{-1} even with annealing temperatures above 200^0C for a thickness of 300 nm. On the other hand silver nanoparticles with thin-film features below 200 nm and at temperatures above 300^0C show high conductivity (Fuller S.B., et al, 2002) due to large particle size or presence of strong stabilizers (Wu Y., et al, 2007). These films, however, exhibit significant porosity.

If silver nanoparticles form strong bonds with organic stabilizing agents they may require high processing temperatures to break these bonds. However, alkylamines are claimed to have weaker interactions with silver which lead to conductive layers at low temperatures. In the work of Li Y., et al., they used a precursor of silver (I) acetate solution which is reduced by phenylhydrazine in the presence of a stabilizer (1-dodecyl-amine) in toluene at temperatures as low as 120-140^0C. The high conductivity and long term stability are in crucial importance in the field of electronic circuit manufacturing. Their reported electrical conductivity of the spin casted silver films is in the range of 2-4 x 10^4 S cm^{-1} for a 70 nm thick film. The organic TFT built by using these silver source and drain contacts exhibit an average mobility of 0.05-0.08 cm^2 $V^{-1}s^{-1}$ and a current on/off ratio of 10^6-10^7 (Li Y., et al, 2005).

Usually silver salts are known to thermally self-reduce to metallic silver, but this process requires a high temperature (Liu Z., et al, 2005) and strong reducing agents such as $NaBH_4$, hydrazine, and aldehyde. However, these reducing agents would cause a rapid reduction of silver salt solution with uncontrolled precipitation (Wu Y., et al, 2007).

Wu Y., et al, reported the solution deposition of silver films without a separate synthesis of nanoparticles. Their method is the deposition by using a solution of a silver (I) acetate, an organoamine (e.g., ethanolamine), and a long-chain carboxylic acid (oleic acid) in an alcohol solvent (n-butanol). They obtained a conductivity about 1.0-2.0 x 10^3 Scm^{-1} by annealing in air at 200°C for 10 min or a conductivity of about > 10^4 S cm^{-1} at 150^0C by increasing the annealing time to ~45 min (Wu Y., et al, 2007). With the acid

additive they reduced the crystalline domains present in the films which lead to low conductive films. The TFT device of a bottom-gate, bottom-contact structural configuration were built on an n-doped silicon wafer using silver source/drain electrodes generated from the silver acetate solution and a spin coated organic channel semiconductor. The obtained FET mobility from this device is reported as 0.10-0.15 cm^2 V^{-1} s^{-1} with a current of on/off ratio in the range of 10^7 (Wu, Y., et al, 2007). As a comparison of TFTs with vacuum-deposited silver electrodes which show a mobility of ~0.06 cm^2 V^{-1} s^{-1} with a current of on/off ratio in the range of 10^6-10^7, the deposition method of Wu Y., et al., was successful. However all these deposition methods use organic materials and show way less mobility values compared to methods using inorganic precursors.

In this study our approach is the deposition of the silver metal films at low temperature from new ink chemistry. Ag_2O is chosen as a precursor since the binding energies of AgO_x are very low and it gradually decomposes into silver islands at a temperature of 160^0C at atmospheric pressure. Previously silver nanoparticles were produced by the deoxidization of AgO_x films in a hydrogen atmosphere (Tominaga J., 2003). This study is concentrated on the deposition of thin films of silver with Ag_2O as the reagent for precursor formation. For this purpose, smooth and conductive films are necessary.

Many compounds of silver are insoluble in water, but the brown solid, Ag_2O, is soluble in alkali solutions such as concentrated NH_3 (aq) forming complexes of $[AgNH_3]^+$ and $[Ag(NH_3)_2]^+$. These complexes may be readily decomposed at low temperatures (150^0C) to silver metal.

Experimental

The deposition of silver metal thin films by spin coating method is achieved via the reduction of silver (I) oxide solution to silver metal. The precursor solution is prepared in the concentrations of 0.05 M and 0.1 M from Ag_2O (s) which is dissolved in concentrated aqueous ammonia. The freshly prepared solution is directly spin coated at a rate of 3000 rpm for 30 s which results in metallic color films. The temperature used between consecutive coats is 120^0C on a hot plate for 30 min.

The substrates used for the deposition are silicon, which has a 1700-Å thick thermally evaporated SiO_2 layer on top of it. Substrates are cleaned at 45^0C for 60 min in an ultrasonic bath of containing Conrad 70 detergent. The clean substrates are rinsed with millipore water and dried by blowing nitrogen gas on them.

The deposited films are characterized with a Siemens (Bruker) D5000 X-ray diffractometer (Cu radiation) and a Multimode^{TM} atomic force microscopy, which is used in contact mode for the identification of the surface morphologies.

Results and Discussion

The films annealed at 120^0C on a hot plate are silver metal; no additional annealing is required. The identity of the films as silver metal is confirmed by the X-ray diffraction data shown in Figure 4.1. From this figure, the peaks of silver metal and the substrate are confirmed. The deposited silver films are around 98 nm thick, which are obtained by 10 consecutive coats via spin coating; they do not show any observable conductivity by simple probing. The overall reaction leading to deposition of the silver film is shown in reaction 4.1.

$$Ag_2O\ (s) + NH_3\ (aq) \longrightarrow 2Ag(s) + NH_3\ (aq) + 1/2O_2\ (g) \qquad 4.1$$

As a reference, the silver (I) oxide (Ag_2O) powder as bought is annealed at 200^0C for 2 h and 300^0C for 2 h in air but it is seen from the X-ray peaks that the silver (I) oxide did not turn to silver metal at all.

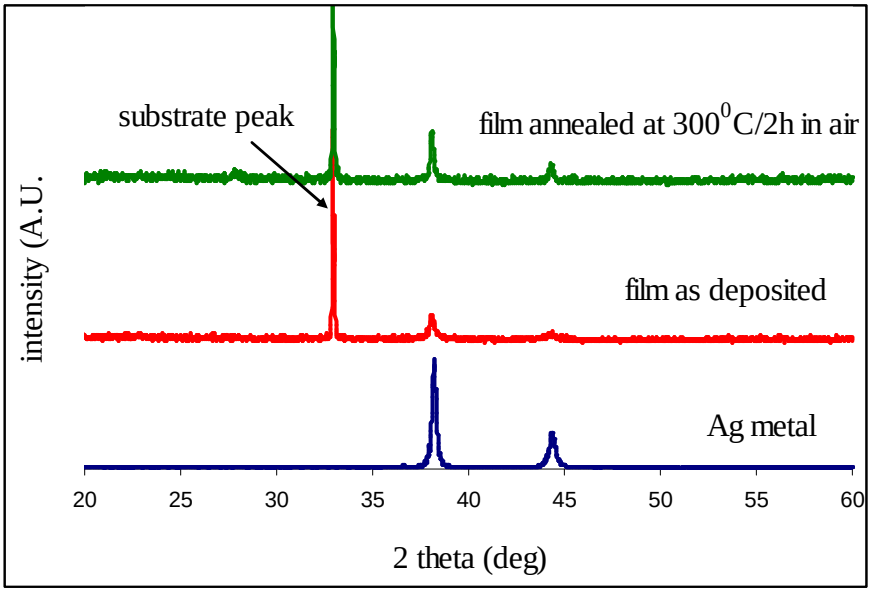

Figure 4.1 Powder X-ray diffraction peaks of the film as deposited (120^0C) and annealed at 300^0C for 2 h in air.

The AFM images of the silver films are seen in Figure 4.2, Figure 4.3 and Figure 4.4. The film in Figure 4.2 is post-annealed in air at 200^0C for 2 h. The films in Figure 4.2 and 4.3 exhibit surface roughnesses of approximately 21.3 nm and 28.3 nm respectively. The film in Figure 4.2 is post-annealed in air at 200^0C for 2 h where the film shown in Figure 4.3 is post-annealed in air at a temperature of 300^0C for 30 min. In the next figure (Figure 4.4) the silver film shown is quite rough with a surface roughness of

~44 nm. The film is quite granular and discontinuous. The silver film in this figure is annealed in air at 300^0C for 2 h followed by a nitrogen atmosphere anneal at 300^0C for 2 h 30 min. As a comparison between those films in Figures 4.2, 4.3 and 4.4 the higher the annealing temperature the rougher the film gets. The least rough films are obtained with the film in Figure 4.2 which is annealed at 200^0C. In all these films a granular morphology can be noticed with some dispersed nanoparticles on the surface.

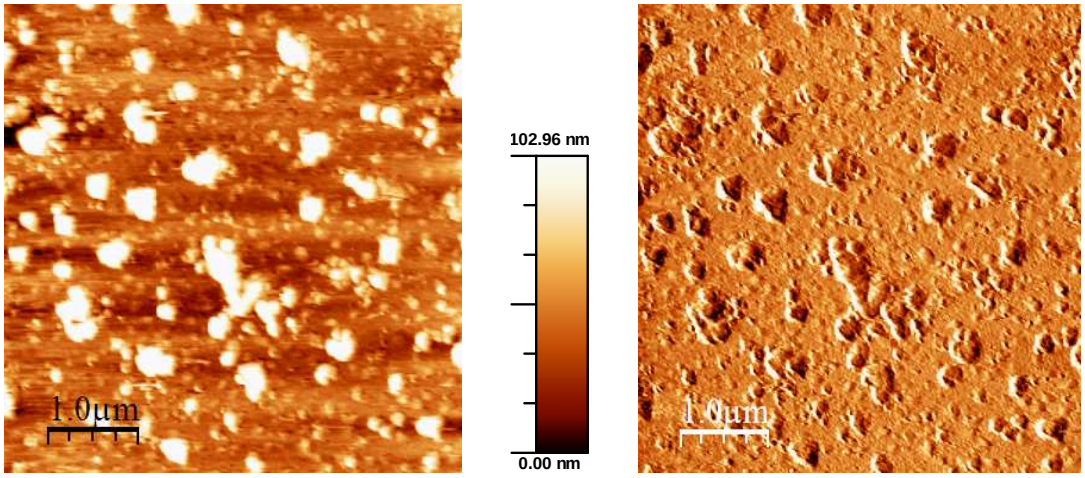

(a) (b)

Figure 4.2 (a) AFM image of the deposited silver films annealed at 200^0C for 2 h in air (b) the deflection image of the image (a).

As a result there are some challenges in the formation of silver films. First, to be used as a conductor in TFT applications the film morphology needs to be improved. Second, the film should be conductive rather than insulating as in our case. To achieve the desired results, the concentration of Ag_2O can be altered, additional Ag salt mixtures can be tested to prevent nucleation, and the effects of spin-coating and annealing process parameters can be examined.

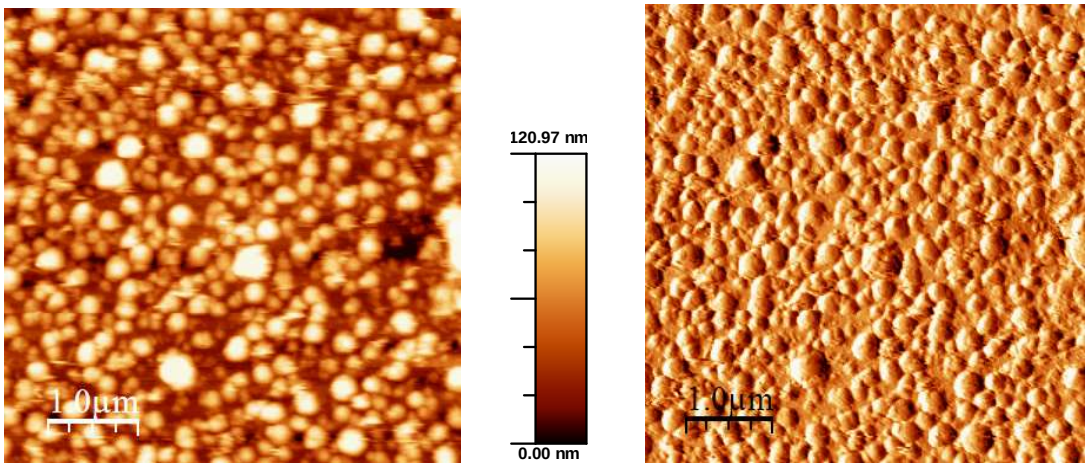

(a) (b)

Figure 4.3 (a) AFM image of the silver films annealed at 300^0C for 30 min in air (b) the deflection image of the image (a).

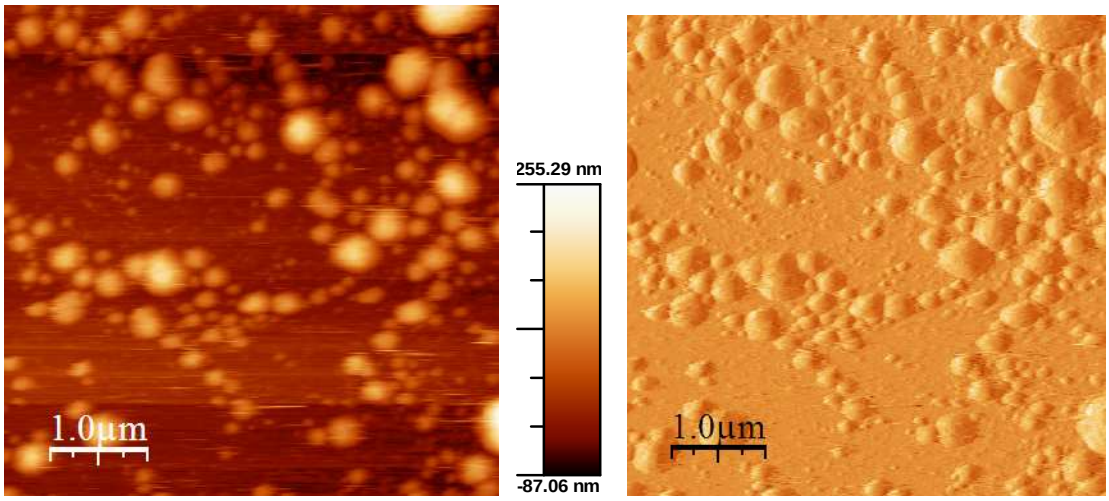

(a) (b)

Figure 4.4 (a) AFM image of the silver films annealed at 300^0C for 2 h in air followed by an anneal at 300^0C for 2 h and 30 min under nitrogen atmosphere (b) the deflection image of the image (a).

Chapter 5

Summary

By spin coating tin (IV) oxide, and zinc-, antimony-doped tin (IV) oxide, it is possible to obtain crystalline films, near 600^0C. The undoped SnO_2 film is too conductive to be used as a channel layer in a TFT, at least with the dielectric materials available for study. In the zinc-doped SnO_2 film, the conductivity is decreased significantly, here, the resulting trap densities and morphology are not conducive to realizing a functioning TFT.

Considering the morphology observed in the SEM images, the lack of device performance is not surprising. It is known that porous and inhomogeneous films can have low mobilities and low carrier concentrations. A high chlorine concentration present in the precursor solution may be equated with an unintentionally high mineral acid content, and probably results in decreased tin polymerization. The as-deposited film therefore exhibits a significant halide salt character rather than a well-bonded hydroxide network. Finally, early nucleation of dehydrated SnO_2 species during precipitation may prevent monolithic gel condensation. As a result, these effects are capable of contributing to the granular morphology seen in SEM images and reflected in limited TFT operation.

ZTO thin films deposited from a single source precursor have demonstrated limited field effect in TFT structures. Device performance appears to be trap dominated, and SEM images suggest morphological contributions as well. Potential changes to solution precursors include higher Zn concentrations, enhanced chlorine removal steps, changes to the soluble tin source, and modifications to the hydroxide precipitation reaction.

In Chapter 3, the nitrogen atmosphere deposition of Cu_2O films is explained. The deposition is performed with the UV decomposition of the films at around room temperature (35^0C). The challenge was to improve the morphology of the films. However the smoothest films are obtained by both UV exposure between coats and a post-deposition anneal with UV light. We can conclude that the current cuprous oxide films need to be densified, and in the future films should be much smoother and free of

porosity. The limitation with current cuprous oxide deposition chemistries has been identified as poor polymerization in the precursor solution.

The solution deposition of the silver films at temperatures as low as 120^0C is discussed. It is a promising result since a post anneal at higher temperatures not needed to deposit these films, providing a means for use of a variety of substrates including dielectrics, metals, plastics etc. If the deposited films were sufficiently conductive and smooth, they could be used as a conductor in a thin film transistor or as a mechanical element in a microelectromechanical device.

BIBLIOGRAPHY

1. Anderson J.T., et al,' Solution-Processed HafSOx and ZircSOx Inorganic Thin-Film Dielectrics and Nanolaminates', *Adv. Funct. Mater*. in press.

2. Ando E., Miyazaki M., 2001, 'Moisture resistance of the low-emissivity coatings with a layer structure of Al-doped ZnO/Ag/Al-doped ZnO', *Thin Solid Films*, **392**, 289.

3. Beensh-Marchwicka G., et al, 1982, 'Effect of the oxygen pressure during sputtering on the properties of thin copper oxide (CuO_x) films', *Thin Solid Films*, **88 (1)**, 33.

4. Bilgin V., et al, 2004, 'The effect of Zn concentration on some physical properties of tin oxide films obtained by ultrasonic spray pyrolysis', *Materials Letters*, **58**, 3686.

5. Brinker C.J., Scherer G.W., 1990, 'Sol-gel Science, The Physics and Chemistry of Sol-Gel Processing', Academic Press, San Diego.

6. Buljan A., 2001, 'Color and conductivity in Cu_2O and $CuAlO_2$: A theoretical analysis of d^{10}.... d^{10} interactions in solid-state compounds', *Chem. Mater*., **13**, 338

7. Calvert P., 2001, 'Inkjet printing for materials and devices', *Chem. Mater*., **13**, 3299.

8. Cava R.J., et al, 1994, '$GaInO_3$: A new transparent conducting oxide', *Appl. Phys. Lett*. **64**, 16.

9. Chiang H.Q. et al, 2005, 'High mobility transparent thin-film transistors with amorphous zinc tin oxide channel layer', *Applied Physics Letters*, **86**, 013503.

10. Efremov V.N., et al, 2002, 'Synthesis of cement-containing nickel-copper catalytic systems using formic acid aqueous solutions', *Russian Journal of Applied Chemistry*, **75 No 5**, 745.

11. Fuller S.B., et al, 2002, 'Ink-jet printed nanoparticle microelectromechanical systems', *J. Microelectromech. Syst.*, **11**, 54.

12. Galwey A.K., et al, 1974, 'Thermal decomposition of three crystalline modifications of anhydrous copper (II) formate', *The Journal of Physical Chemistry*, **78 No 26**, 2664.

BIBLIOGRAPHY (Continued)

13. Ginley D. S., Bright C., 2000, 'Transparent conducting oxides', *MRS Bulletin*, **25(8)**, 15.

14. Gordon R.G., 1996, 'Preparation and properties of transparent conductors', *Mat. Res. Soc. Symp. Proc*., **426**, 419.

15. Gray, C., et al, 2001,' Screen printed organic thin film transistors (OTFTs) on a flexible substrate', *Proceedings of SPIE*, **4466**, 89

16. Hartnagel H.L., Dawar A.L., Jain A.K., Jagadish C., 1995, 'Semiconducting Transparent Thin Films', Institute of Physics Publishing Bristol and Philadelphia.

17. Hong D., et al, 2006, 'Zinc tin oxide thin-film transistors via reactive sputtering using a metal target', *J. Vac. Sci. Technol. B*., **24 (5)**, L23.

18. Hosono H. et al, 1996, 'Working hypothesis to explore novel wide band gap electrically conducting amorphous oxides and examples', *J. Non-Cryst. Solids*, **198-200**, 165.

19. Hosono H., 2006, 'Ionic amorphous oxide semiconductors: Material design, carrier transport, and device application', *J. of Non-crystalline solids*, **352**, 851.

20. Housecroft C.E., Sharpe A.G., 2001, 'Inorganic Chemistry', Pearson Education Limited.

21. Jarzebski Z.M., 1982, 'Preparation and physical properties of transparent conducting oxide films', *Phys. Status Solidi A*, **71**, 13.

22. Kluth O., et al, 2003, 'Magnetron sputtered zinc stannate films for silicon thin film solar cells', *Third World Conf. Photovolt. Energy Conversion*, **2**, 1800.

23. Li Y.,et al, 2005, 'Facile Synthesis of Silver Nanoparticles Useful for Fabrication of High-Conductivity Elements for Printed Electronics', *J. Am. Chem. Soc.*, **127**, 3266.

24. Liu, Z., et al, 2005,' Inkjet-printed silver conductors using silver nitrate ink and their electrical contacts with conducting polymers', *Thin Solid Films*, **478**, 275.

25. Luzeau P., et al, 1990, 'Copper oxide thin-film growth using an oxygen plasma source', *J. Vac. Sci. Technol. A*, **8 (6)**, 3938.

BIBLIOGRAPHY (Continued)

26. Minami T., et al, 1995, 'Properties of transparent zinc-stannate conducting films prepared by radio frequency magnetron sputtering', *Journal of Vacuum Science & Technology, A: Vacuum, Surfaces, and Films*, **13 (3, Pt. 1)**, 1095-9.

27. Minami T., 2005, 'Transparent conducting oxide semiconductors for transparent electrodes', *Semicond. Sci. Technol*., **20**, S35.

28. Mitzi D.B., 2004, 'Solution-processed inorganic semiconductors', *J. Mater. Chem.*, **14(15)**, 2355.

29. Mitzi D.B., et al, 2006, 'High-Mobility p-Type Transistor Based on a Spin-Coated Metal Telluride Semiconductor', *Adv. Mater.*, **18**, 2448.

30. Mohamed M.A., et al, 2004, 'Kinetic and thermodynamic studies of the nonisothermal decomposition of anhydrous copper (II) formate in different gas atmospheres', *Thermochimica Acta*, **411**, 13.

31. Munnix S., Schmeits M., 1982, 'Surface electronic structure of tin (IV) oxide (110)', *Solid State Commun*., **43**, 867.

32. Nair M.T.S., et al, 1999, 'Chemically deposited copper oxide thin films: structural, optical and electrical characteristics', *Applied Surface Science*, **150**, 143.

33. Narsimlu N., Sastry G.S., 1996, 'Optical properties of anhydrous copper (II) formate single crystal', *Solid State Communications*, **100 No 10**, 687.

34. Pankov Ju. D., et al, 1978, Izv. Vuzov. Fiz. **3**,126.

35. Pierret R.F., 1996, 'Semiconductor Device Fundamentals', Addison-Wesley Publishing Company, Inc.

36. Porat, O., Riess, I., 1995, 'Defect chemistry of $Cu_{2-y}O$ at elevated temperatures. II. Electrical conductivity, thermoelectric power and charged point defects', *Solid State Ionics*, **81**, 29-41.

37. Portier J., et al., 2004, 'Thermodynamic correlations and band gap calculations in metal oxides', *Progress in Solid State Chemistry*, **32**, 207.

38. Presley R.E., et al, 2004, 'Tin oxide transparent thin-film transistors', *J. Phys. D: Appl. Phys.*, **37**, 2810

BIBLIOGRAPHY (Continued)

39. Rai B.P., 1988, 'Cuprous oxide solar cells: a review', *Sol. Cells*, **25**, 265.

40. Rakhshani A. E., 1986, 'Preparation, characteristics and photovoltaic properties of cuprous oxide- a review', *Solid-State Electron.*, **29**, 7.

41. Ristov M., et al, 1985, 'Chemical deposition of copper(I) oxide thin films', *Thin Solid Films,* **123**, 63.

42. Sahm H. et al, 2004, 'Oxidation behaviour of thin silver films deposited on plastic web characterized by spectroscopic ellipsometry (SE)', *Thin Solid Films*, **455-456**, 819.

43. Sato H., et al, 1993, 'Transparent conducting p-type NiO thin films prepared by magnetron sputtering', *Thin Solid Films*, **236,** 27.

44. Srinivasa M.N., Jawalekar S.R., 1983, 'Characterization of antimony-doped tin oxide films for solar cell applications', *Thin Solid Films*, **108**, 277.

45. Stathatos E., et al, 2000, 'Photocatalytically deposited silver nanoparticles on mesoporous TiO_2 films', *Langmuir*, **16**, 2398.

46. Toledo-Antonio J.A., 2003, 'Thermal stability and structural deformation of rutile SnO_2 nanoparticles', *Journal of Solid State Chemistry*, **174**, 241.

47. Tominaga J., 2003, 'The application of silver oxide thin films to plasmon photonic devices', *J. Phys. Condens. Matter*, **15**, R1101.

48. Trotman-Dickenson A.F., 1973, 'Comprehensive Inorganic Chemistry', Pergamon, Oxford, **3**, 16–39.

49. Vigil E., et al., 2005, 'Preparation of photoelectrodes with spectral response in the visible without applied bias based on photochemically deposited copper oxide inside a porous titanium dioxide film', *Thin Solid Films*, **489**, 50.

50. Wu Y., et al, 2005,' High-Performance Organic Thin-Film Transistors with Solution-Printed Gold Contacts', *Adv. Mater*., **17**, 184

51. Wu Y., et al, 2007,' A Simple and Efficient Approach to a Printable Silver Conductor for Printed Electronics', *J. Am. Chem. Soc*., **129**, 1862.

BIBLIOGRAPHY (Continued)

52. Young D. L., et al, 2002, ‘Growth and characterization of radio frequency magnetron sputter-deposited zinc stannate, Zn_2SnO_4, thin films’, *Journal of Applied Physics*, **92 (1)**, 310-319.